UNIVERSITY OF OSLO
Department of Physics

Thermoelectric hybrid materials

Master thesis
(60 credits)

by

Nataliya Kochergova

May 2013

Thermoelectric hybrid materials

by

Nataliya Kochergova

Master thesis

Materials, Energy and Nanotechnology- Department of Physics
University of Oslo

May 2013

Preface

This thesis is based on practical work, as well as research in relevant science literature. The practical part of the work was conducted in the Research Park, the MiNaLab, and the Chemistry building in the University of Oslo. Most of the work was done during the fall 2012 and the spring 2013 semesters.

I would like to thank everyone who contributed to this project, first and foremost my supervisors. The ideas of the project were suggested to me by Terje Finstad, Ole Bjørn Karlsen and Johan Taftø, who later all became my supervisors. I would also like to thank Anette Eleonora Gunnæs, who took over Johan Taftø's place as supervisor within the time period of my studies. This project would not have been completed without their assistance with experiments and helpful advice and suggestions.

I have also received practical lessons in experimental methods from several other people, and want to thank them for taking time to give me instructions and teach me the skills essential to my thesis. Stefano Rubino taught me how to use the TEM. Ramon Schifano taught me how to use the temperature-dependent Hall instrument. Victor Bobal taught me the general knowledge about the cleanroom. I also received a lot of method-related advice from Xin Song, and practical lessons in a myriad of methods from Kjetil Valset.

Nataliya Kochergova

Oslo, May 2013

Abstract

Polycrystalline silicon sample was prepared by crushing, ball-milling and hot-pressing a single crystalline silicon wafer. The polycrystalline product was characterized with optical microscopy, TEM and SEM. Its porosity was found to be 15-22%.. The following thermoelectric properties of both the single crystal silicon and the polycrystalline sample were determined: thermal conductivity, electrical resistivity, Hall mobility, carrier concentration and Seebeck coefficient. It was found that porosity and polycrystallinity decrease thermal conductivity only slightly. They also decrease the Seebeck coefficient, carrier concentration, carrier mobility and electrical conductivity.

Literature on effective medium theory (EMT) is reviewed. It is discovered that the apparent validity of an effective medium theory depends strongly on the model that is chosen for description of the composite. Careful microstructural characterization is necessary for successful use of an EMT. A new way of studying porosity in the context of EMT is suggested.

Table of contents

f

List of Figures

List of Tables

Chapter 1

Introduction

Every year, the amounts of oil and gas are decreasing, while the energy demand is increasing. It is also expected to increase in the following years [1]. These non-renewable resources are used inefficiently. For example, only a quarter of the energy in gasoline goes to power and move the car, while the rest gets converted to heat [2]. If some of the energy wasted as heat could be put to use, we would be one step closer to reduced pollution, reduced greenhouse gas emission and the solution to future energy demands. Thermoelectric devices could be one way to do it. They can be used to convert temperature gradients into useful electricity. The idea of using the thermoelectric effects to extract electricity has been around for more than a century, but progress has been slow – the thermoelectrics available are not efficient enough to be competitive in the energy market. Since the 1990s, a new promising idea appeared in the field: nanostructuring the materials increases their efficiency. To nanostructure a material means to incorporate grains and phases that have at least one dimension on the nanoscale (<100 nm). To develop this field and achieve good results, more research is needed. This master thesis is involved in that collective effort. The focus of this thesis is effective medium theory (EMT), and how it can be utilized to model thermoelectric properties. EMT is a model that expresses effective properties of a composite material, as a function of the properties and volume fractions of its components. The text will elucidate what research has been done in this particular area. It will also describe the author's own measurements of thermoelectric properties of nanostructured materials. The resulting measured effective properties will be compared to existing effective medium theory

This introductory chapter will describe the history of thermoelectricity, and some previous research. It will also briefly describe the thermoelectric effects, how thermoelectric efficiency is quantified and the current situation on thermoelectric materials. The last part of the chapter will describe the goal of the master thesis and its practical work in more detail.

1.1 History of thermoelectricity and previous work [3]

There are three thermoelectric effects. The first of them, the Seebeck effect, was discovered in 1821, by T. J. Seebeck, a Baltic German physicist. He connected two wires of different metals

to each other, and their free ends were attached to the terminals of a voltmeter. Heating the junction between the wires produced a small voltage, detectable by the voltmeter.

In 1834, J. Peltier, a French watchmaker, discovered another thermoelectric effect, named the Peltier effect after his name. It was demonstrated using the same setup used by T. J. Seebeck, although this time, an electric current was run through the connected wires. It produced heating or cooling at the junction, depending on the direction of the current.

It wasn't until 1855 that these two effects were recognized as connected. W. Thomson discovered the relationship between the Seebeck and the Peltier coefficients, by using thermodynamics. He also discovered the Thomson effect, which is a reversible heating or cooling within a homogenous conductor, when both a current and a temperature gradient are present.

In principle, the Seebeck effect could be used for generating electricity, but no materials were found that could provide efficient energy conversion. In the 1950s, semiconductors came into use as thermoelectric materials. Bi_2Te_3 was the most promising material of that time. It was mixed with Sb_2Te_3 at various concentrations, in order to optimize the final efficiency at specific temperatures [4]. This allowed Peltier refrigerators and thermoelectric generators to be made, but they had only enough efficiency for special applications in space missions, laboratory and medical equipment [5].

Only very small improvements have been achieved in the efficiency of thermoelectric generators between 1950s and the 1990s. The devices made out of the bulk thermoelectric materials operated at 5-6% conversion efficiency. Attempts to increase the efficiency revolved around creating isostructural solid solution alloys [6]. Two examples of such an alloy are p-type $Bi_{2-x}Sb_xTe_3$ and n-type $Bi_2Te_{3-x}Se_x$, which are better than the parent system Bi_2Te_3. Alloys based on PbTe, GeTe, SnTe and SiGe were also explored [4].

In the early 1990s, the US Department of Defense became interested in thermoelectric devices, and encouraged a new round of research. It had good results. Research diverged into two directions: advanced bulk materials, and low-dimensional or nanostructured materials. The advanced bulk material group includes materials containing heavy rattling atoms, such as skutterudites and clathrates [5,4], as well as materials with large complex unit cells, such as Zintl phases.

It was theoretically predicted that nanostructuring would lead to better thermoelectric efficiencies, and theories were followed by experiments. It turns out that nanostructured thermoelectric materials do have larger conversion efficiencies. In 2009, all top performing materials were nanostructured [6].

1.2 Introductory theory

Some important concepts introduced in the text above will now be briefly explained. First of all, the three thermoelectric effects. They occur because charge carriers can transport heat. When a metal or semiconductor is subjected to a temperature gradient ∇T, the carriers move from the hot end towards the cold end, as if they were free gas molecules [7]. If the material is an n-type semiconductor, electrons are the charge carriers that move towards the colder side. If the material is a p-type semiconductor, it is holes. The Seebeck effect is the voltage that occurs when a piece of isolated conducting material has a temperature difference ΔT between its ends. This is called the absolute Seebeck effect. The absolute Seebeck coefficient is the potential difference drop between the ends, per degree temperature difference, or [7]

$$\alpha = \frac{dV}{dT}$$

This effect needs no running electric current, only a temperature difference between the ends of the conductor piece. However, this way of measuring the Seebeck coefficient is not practical, and there is another way to visualize the Seebeck effect. One can look at two different conductors, A and B, connected together and subjected to a temperature difference ΔT at the junctions, as shown in figure 1.1. This setup is called a thermocouple. A voltage V appears between the ends. This is called the relative Seebeck effect. It results from the individual absolute Seebeck effects inside each conductor. The relative Seebeck coefficient is defined as follows:

$$\alpha_{AB} = \frac{V}{\Delta T} = \alpha_A - \alpha_B$$

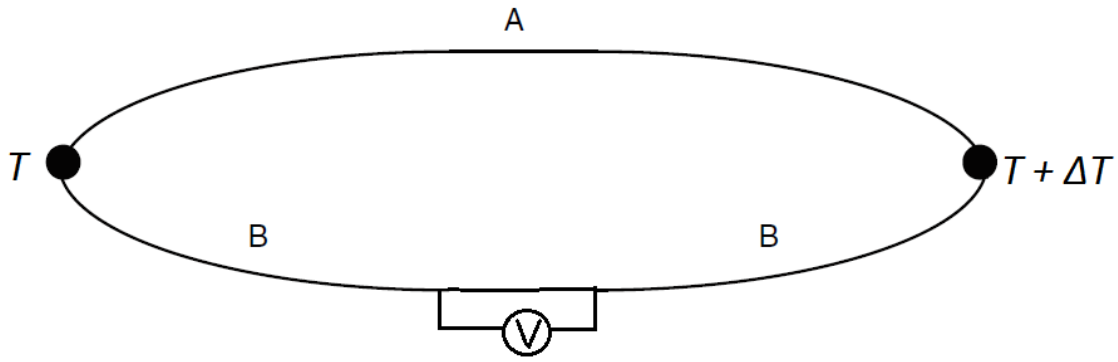

Figure 1.1: The setup for observation of the Seebeck effect. Conductors A and B are connected, and subjected to a temperature difference at the junctions. (Borrowed from [3], and altered according to [8]).

The sign of the relative Seebeck coefficient depends on the direction of the current. The relative Seebeck coefficient is equal to the absolute Seebeck coefficient of one conductor, if the other one is a superconducting material.

The Peltier effect is the reversible loss or gain of heat, when electric current crosses a boundary between two differing conductors, as shown in the figure 1.2.

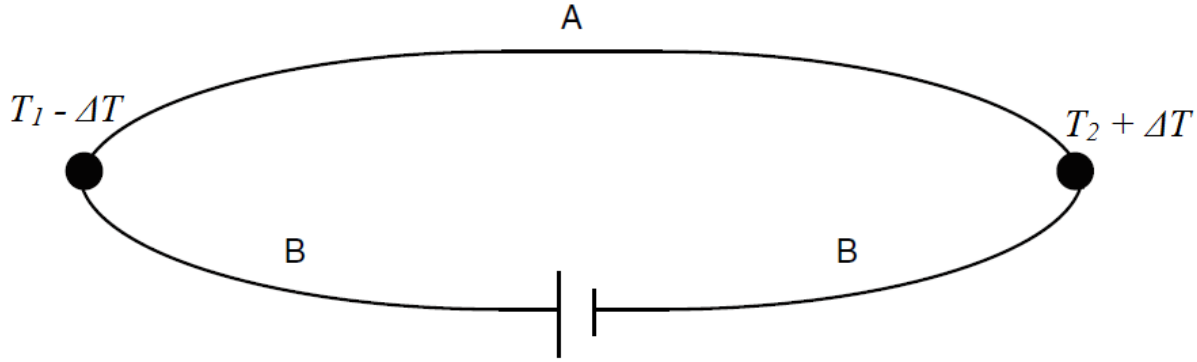

Figure 1.2: The setup for observing the Peltier effect. Two different conductors, A and B are connected as shown, and a source of current is placed between the free ends of conductor B. (Borrowed from [3], and altered according to [8]). Heating or cooling is observed at the junctions between A and B.

The relative Peltier coefficient π_{AB} can be written as follows:

$$\pi_{AB} = \frac{q}{I},$$

where q is the rate of cooling or heating at each junction, and I is the current. The Peltier effect can also occur within inhomogenous conductors, at their concentration gradients. It can occur at phase interfaces within a multiphase material as well.

The Thomson effect is the reversible change of heat content within a single homogenous conductor, subjected to a temperature gradient and an electric current. The electrical carriers absorb heat, when they flow in the direction that is against the temperature gradient. They give off heat, when flowing in the direction of the temperature gradient. Thomson coefficient, β, can be expressed as in the following equation:

$$\beta = -\frac{q}{J\,\nabla T}$$

Here, q is the rate of heat flow, J is the electric current density, and ∇T is the temperature gradient.

The thermoelectric effects themselves are reversible, and don't increase entropy in the thermocouple or the environment. However, in real situations, conduction of electricity is often accompanied by irreversible effects, such as electrical resistance and thermal conduction [3].

The second essential concept about thermoelectric materials is the figure of merit. The efficiency of a thermoelectric material is usually described by this number, and it is written as ZT, where T is the temperature in Kelvin [6]. This is a dimensionless number. A good, useful thermoelectric material has a figure of merit larger than unity; and a very good thermoelectric material has a figure of merit much larger than unity. ZT depends on several of the material's properties, written in the following equation:

$$ZT = \frac{\alpha^2\sigma}{\kappa}T$$

σ is the electrical conductivity, α is the Seebeck coefficient, κ is the thermal conductivity and T is the absolute temperature in Kelvin. To have a large figure of merit, the material needs to have high power factor ($\alpha^2\sigma$) and low thermal conductivity. Large power factor means that a large voltage and a large current are generated by the Seebeck effect [6].

It is important to note that the dimensionless figure of merit rises with temperature, even if *Z* alone does not, and the challenge is to achieve *ZT* larger than one at room temperature.

1.3 The definition and description of the master thesis work

Today, thermoelectric materials are unfortunately not good enough to affect the trends in global energy production and use. They don't yet contribute to the solution of our energy problems. There are still many areas of knowledge about thermoelectric materials that haven't been properly researched, studying which would take us closer to effective materials. Latest attempts to improve thermoelectric materials have been about nanostructuring them. Nanostructuring can reduce the lattice thermal conductivity of the material by increasing phonon scattering, and possibly increase *ZT* by introducing the energy filtering effect. One way to nanostructure is to create hybrid materials. Hybrid materials are composites of two moieties on the nanometer scale or molecular level [9]. The aim of such mixing of constituents is to produce a material that inherits their advantageous properties, but lacks their faults [10]. In such a way, ordinary materials can be mixed to produce new materials with unordinary properties. Effective medium theory is a way to model the thermoelectric properties of such mixtures. One can use this model to design new efficient thermoelectric materials. A good model can show us how much of each phase are to be mixed, and what properties the mixed phases should have.

This master thesis will contribute to understanding of hybrid thermoelectric materials and the EMT. It will review the published scientific work done on effective medium theory in the context of thermoelectricity, as well as published work about nanostructured thermoelectric materials. The following practical work will also be done. A solid polycrystalline material will first be synthesized. It will have two constituents: grains of silicon and empty space or air. The material's microstructure will be characterized using the optical microscope, the transmission electron microscope (TEM) and the scanning electron microscope (SEM). The density and empty space content of the sample will be measured. Then, the sample's effective resistivity, effective Hall voltage, effective carrier concentration, effective Seebeck coefficient and effective thermal conductivity will be measured. Then the data will be analyzed and compared with data of single crystalline silicon, and existing effective medium theory.

Chapter 2

Theory

This chapter will explain the physics and theory behind thermoelectric materials beyond what has already been said in chapter 1. It will also delve into theory of the other fields that are important to understand the work conducted for this master thesis.

2.1 The figure of merit

The figure of merit *ZT* is a measure of how efficient a thermoelectric material is. It is connected with the thermoelectric conversion efficiency (TCE) as shown in the following equation [11]:

$$\text{TCE} = \frac{T_h - T_c}{T_h}\left(\frac{\sqrt{1+ZT_{av}}-1}{\sqrt{1+ZT_{av}}+\left(\frac{T_c}{T_h}\right)}\right)$$

T_c and T_h are the two temperatures which give rise to the thermal gradient, cold and hot. T_{av} is their average. A high *ZT* means a high TCE.

2.1.1 The properties in the figure of merit

There are three important properties in the equation for the figure or merit *ZT*: thermal conductivity κ, Seebeck coefficient α and electrical conductivity σ.

Thermal conductivity κ is defined in the following equation [3]:

$$\kappa = -\frac{qL}{A\,\Delta T}$$

Here, q is the rate of heat flow through a sample with a fixed cross-sectional area A, length L, and a temperature difference of ΔT between the two ends. The higher the rate of heat flow through the length of the sample, the higher the κ. A metal or a semiconductor has a concentration of electrons, as well as a concentration of lattice phonons. The latter are vibrations of the lattice. Both electrons and phonons transport thermal energy. Thus, thermal conductivity is a sum of carrier thermal conductivity κ_e and lattice thermal conductivity κ_{latt}.

The Seebeck coefficient is an important factor in the equation for the figure of merit. It is squared in the equation, which makes it more influential than the other two factors. This sometimes allows a lower electrical conductivity to be tolerated, as long as the Seebeck coefficient is high enough to counteract it. The equation of the Seebeck coeffient is described in detail in chapter 1.

Electrical conductivity is a measure of how easy is it to set charge carriers in directed motion within a material. The bigger the conductivity of a material, the smaller electric field is needed to produce a specific current density. It is defined in the following equation:

$$\sigma = \frac{IL}{VA}$$

Here, I is a current that goes through a sample with a constant cross-section A and length L, and V is the voltage between the two ends. Electrical conductivity is related to resistivity ρ through this equation:

$$\sigma = \frac{1}{\rho}$$

2.1.2 The fundamental challenges of increasing the figure of merit

In some ways, the task of increasing the figure of merit seems simple: one only needs to increase σ and α, and decrease κ. However, the properties ZT depends on are connected in such a way that raising one will lower the other. First, there are the conflicting dependencies of α and σ on carrier concentration n (or p, if the material is a p-type semiconductor). Second, there are the dependencies of α and σ on carrier mobility μ. Third, the conflicting dependencies of κ and σ on the presence of defects in the crystal. Fourth, the inevitable increase of κ_e with σ. There is also the problematic bipolar effect. All the challenges will now be explained.

To increase the power factor, both the Seebeck coefficient and the electrical conductivity need to be increased. This has some fundamental limitations. For metals and degenerate semiconductors, the Seebeck coefficient is given by this equation:

$$\alpha = \frac{8\pi^2 k_B^2}{3eh^2} m^* T \left(\frac{\pi}{3n}\right)^{2/3}$$

Here, n is the carrier concentration, and m^* is the effective mass of the carrier. A high α needs a low carrier concentration, and a high effective carrier mass. The electrical conductivity is expressed as follows, and it is obvious that it needs a large carrier concentration, which conflicts with requirements for a large α:

$$\sigma = ne\mu_e + pe\mu_h \qquad \text{(general conductivity)}$$

$$\sigma = ne\mu_e \qquad \text{(for n-type)}$$

The ZT is optimized typically at carrier concentrations 10^{19} to 10^{21} carriers per cm^3 [4, 7].

The effective mass m^* is also a conflicting parameter. A large m^* means large α, but it lowers carrier mobility μ, which in turn lowers the electrical conductivity.

Another fundamental challenge is reducing κ without reducing μ and therefore σ. Structural defects scatter phonons and lower thermal conductivity, but they also tend to scatter the charge carriers, lowering the electrical conductivity.

Even when all the above obstacles are overcome, a larger σ can itself be a cause of slight difficulties. While it is good for a higher figure of merit, it increases the electronic contribution to thermal conductivity, κ_e. The effect can be expressed through the equation called the Wiedemann-Franz law: $\kappa_{el} = \sigma LT$. L is the Lorentz number, which is between $1.6 * 10^{-8} V^2/K^2$ and $2.2 * 10^{-8} V^2/K^2$. [12]

The bipolar effect occurs then the material contains carriers of both types, holes and electrons. This lowers the Seebeck coefficient.

2.1.3 The challenge of and strategies for decreasing thermal conductivity

Decreasing the thermal conductivity is a major part of research of high ZT materials. Thermal conductivity can be expressed as in the following equation [7]:

$$\kappa = \frac{1}{3} c v \lambda$$

Here, c is the specific heat, v is velocity of phonons, and λ is mean free path. Therefore, decreasing the mean free path of the phonons is a good strategy. It can be achieved by putting a lot of obstacles in the way of phonons.

These obstacles can take many forms. First, complex crystal structures have enough disorder to scatter phonons, but still have crystallinity that is needed for good electron transport [4]. There are complex bulk materials such as clathrates, skutterudites and Zintl phases. Distorted lattices are also a way to scatter phonons [11]. Second, point defects in general (vacancies, substitutions, and interstitials) scatter phonons due to mass variation, especially short-wavelength phonons. Phonons depend on the lattice to propagate. Once something in the lattice changes from the norm, a phonon with a specific frequency and wavelength can be prevented from propagating in that direction. Solid solution alloying is therefore a good way to limit κ. Unfortunately, solid solution alloying often leads to deterioration of the electronic properties of the material, such as charge carrier mobility, which is the fundamental challenge number three. Third, grain boundaries can also scatter phonons, and nanostructuring is the way to introduce a high grain boundary density.

Porous materials have lower thermal conductivity as well. They contain voids, which are filled with air. Air is a very poor thermal conductor. Because of this, many thermal insulators are made of porous materials [7].

In the case of highly disordered material, a minimum value for lattice thermal conductivity was found for semiconductors and semimetals by Cahill and Pohl [13]. It is around 0.25 – 0.50 W/mK. It is considered the lower limit. When it is reached, other ways of increasing *ZT* need to be utilized.

2.2 Nanostructured thermoelectric materials

In section 2.1.2 the fundamental challenges were stated. There are two potential solutions to these challenges. It could be decoupling the properties by designing the material in a specific way, so that it becomes possible to increase one property without decreasing the other. Another method could be to optimize both properties. For example to find the charge carrier concentration n, at which the power factor $\alpha^2\sigma$ is the largest possible. Nanostructuring can accomplish the problem of decoupling. When the scale of the system decreases, it is theorized that α, σ and κ become possible to vary quasi-independently [5]. Nanostructuring is also a great way to decrease κ.

To decouple α and n, the following things could be done: decrease density of states (DOS), perhaps by introducing resonant states, or by quantum confinement to narrow the DOS [11].

To decouple effective mass m^* and mobility μ, one can change the scattering mechanism from normal acoustic phonon scattering (scattering parameter r = -1/2, and $\mu \propto (m^*)^{-1}$) to ionized defect scattering (r = 3/2, $\mu \propto m^*$).

Decoupling κ_e and σ might not be possible, but the Lorentz number in the Wiedemann-Franz law could be made smaller than the normal value. Such an effect could be achieved by shaping the electronic DOS either as a sharp distribution similar to a Dirac delta function, or a rectangular one.

To overcome the last fundamental challenge, the bipolar effect, one can enlarge the band gap. It would prevent more major carriers from crossing it and forming minor carriers. One could try to increase the ratios m^*_e/m^*_h and μ_e/μ_h for n-type, or m^*_h/m^*_e and μ_h/μ_e for p-type material. This could be done by introducing nanoinclusions that scatter one type of carrier, but not the other [11].

As said earlier, many of these decouplings can be achieved by nanostructuring. There are two types of promising nanostructured materials: host materials containing nanosized inclusions and nanocomposites made up of phases that have low dimensionality [5]. Some of the latter can also be called hybrid materials.

One potential beneficial effect of nanostructuring is the energy-filtering effect. This is due to the ability of the increased number of interfaces to trap and filter out the low-energy charge carriers. Interfaces act like barriers. Only carriers with energy substantially more than the Fermi energy E_F will pass through. This may decouple the electrical conductivity and Seebeck coefficient [5,4]. Usually, this reduces electrical conductivity somewhat, but increases the Seebeck coefficient. That more than compensates for losses in σ and results in enhanced ZT. This effect can happen in both nanocomposite polycrystalline materials, and nanoinclusions embedded in a matrix. Unfortunately, little is known about the mechanism of this effect [11].

Another cause of enhanced ZT is that low dimensionality of grains causes quantum confinement. This effect causes narrow, flat electronic bands, which in turn leads to high effective carrier masses and thus high Seebeck coefficients. Quantum confinement can also help vary α and σ somewhat independently.

As stated earlier, nanostructuring decreases κ_{latt} and can decrease the carrier mobility. To restore mobility to its higher value, one must reconstruct electron transport channels. One way is to align the randomly oriented grains inside a polycrystalline nanocomposite. It is also possible to use modulation doping. This technique involves doping only one phase in a two-phase composite [11]. The minor phase is often the heavily doped one. The undoped matrix phase functions as a high-speed channel for carrier transport. This allows the charge carriers to pass through a material that imposes much less impurity-electron scattering on them.

Another reason why nanostructuring improves *ZT* is that nanostructuring introduces many interfaces. The challenge is to use the increased density of interfaces to scatter phonons more than electrons, lowering κ without lowering σ as much.

Incoherent nanoinclusions can serve as an energy filter for phonons, and lower κ_{latt}. Incoherent nanoinclusions are those which lattice parameter differs strongly from that of the matrix phase. It also has a clear boundary between itself and the matrix phase. Mismatched phonon modes at this boundary leads to phonon scattering. Phonons with a wavelength longer than the inclusion dimensions cannot pass through the inclusions, and are filtered out [11]. Coherent inclusions, on the other hand, have a similar lattice parameter to that of the matrix, and show good lattice alignment with the matrix. Coherent inclusions scatter phonons due to mismatched lattice strain. Unlike incoherent inclusions, the coherent ones don't have a negative effect on electronic transport, and give higher *ZT*. In general, it's preferable for a nanostructured material to have thermodynamically stable, epitaxy-like interfaces between its phases. This would prevent electrons from being scattered off grain-boundaries. It could be done by making the precursor phase spontaneously split into two thermodynamically stable phases [4].

Introduction of resonant states is also a good way to increase *ZT* by decreasing κ. It is typically a phenomenon that happens in filled skutterudites. These materials contain heavy atoms, rattling in the cages formed by the atoms of the host material. This produces local phonons. When a lattice phonon encounters such a local phonon, a small part of their energy is absorbed. The local phonon then goes into an excited state. After a while, it gives back the energy, but only to the lattice phonons with wave vectors incoherent with those of absorbed phonons. The whole process can only happen between local phonons and lattice phonons of similar energies [11].

It would also be useful to induce an energy-filtering effect - preferential scattering of those phonons that contribute to thermal conductivity the most [5]. It was found that a distribution in sizes of nanoinclusions will scatter phonons with energy and mean free path of a wider range, than nanoinclusions of the same size. It is challenging however, because mean free paths of phonons with a specific energy are not known for specific materials [11].

It was also found through calculations and experiments [12], that nanoinclusions with an oblong shape give the material a lower thermal conductivity, than the inclusions with an aspect ratio of 1. An aspect ratio of 2 or ½ is better than 1, and an aspect ratio of 3 or 1/3 is better than 2 or ½.

There are two more effects that makes nanostructuring useful for enhancing the figure of merit: carrier-pocket engineering and semimetal-semiconductor transition [5].

Semimetal-semiconductor transition is an effect that can help us use semimetals as good thermoelectrics. Some semimetals, like bismuth, have a high Seebeck coefficient of electrons. This beneficial effect is ruined by the fact that bismuth also has holes as carriers, which gives a negative contribution to the total Seebeck coefficient. Reducing dimensions of bismuth will decrease the number of quantum states available in that direction. It leads to energy bands splitting: the bottom of the conduction band moves upwards, and the top of the valence band moves downwards, until a band gap appears. This turns the semimetal into a semiconductor, which can be doped to have one dominant carrier type. Thus, bismuth's great electronic properties become available for use.

Carrier-pocket engineering is a concept that is meant to occur in the following structure: a superlattice structure, with one type of carrier quantum confined to a quantum-well region, and another type of carrier (of the same sign) confined to the barrier region. An example of such material is GaAs/AlAs quantum-well superlattice. GaAs quantum wells are populated by Γ-point electrons, and AlAs barriers are populated by X-point electrons.

In general, the properties of a material change when the material is reduced to nanoscale. A semiconductor's optical absorption spectra shift to shorter wavelength. This effect occurs, because the band gap increases while particle size decreases [14]. A nanoparticle will also melt at a lower temperature, and have a lower specific heat.

2.3 Effective-medium theory

Often it is useful to calculate effective properties of composite systems. The composite systems could be aerosols, dust, porous media, or solid composites like wood or a nanostructured thermoelectric. They all consist of many small phases with different properties, which are mixed together in a specific way. Examples of effective properties are effective dielectric constant, effective thermal conductivity and effective electrical conductivity.

Effective medium theory (EMT) is one of the techniques that can help calculate the effective physical properties of composite media. It is a model that averages properties at the mesoscopic scale - an intermediate between continuum macroscoping scale and atomic scale[15]. Other techniques for finding these, besides EMT, are other approximate methods, rigorous bounding techniques, and numerical methods. However, EMT is considered to be the most powerful approach [16]. The two most common EMTs are the Maxwell-Garnett relation and the Bruggeman EMT. There can be, in fact, an infinite number of EMTs. Many new predictive equations have been developed based on the effective medium theory since its creation, and they help research in many fields of science [16].

2.3.1 The Maxwell-Garnett relation

One of the oldest EMTs is the Maxwell-Garnett mixing rule, published in 1904. It was developed for optical properties. It was based on the Clausius-Mossotti relation, which in turn was based on the Lorenz local field relation [15]. During the derivation, this EMT focuses on an individual particle and how it is affected by a local electric field, which is different from the averaged electric field inside the material. This EMT can describe many electromagnetic effective properties, but here the effective dielectric constant of a composite will be described. Imagine a material where spherical inclusions with dielectric constant ε_i are embedded inside a matrix with dielectric constant ε_{mat}. Inclusions take up the volume fraction f_i of the material. The effective dielectric constant ε_{eff} is then expressed in the following equation:

$$\left(\frac{\varepsilon_{eff} - \varepsilon_{mat}}{\varepsilon_{eff} + 2\varepsilon_{mat}}\right) = f_{inc}\left(\frac{\varepsilon_i - \varepsilon_{mat}}{\varepsilon_i + 2\varepsilon_{mat}}\right)$$

There are many issues with the model. It works best when applied to dilute composite systems. It is best for describing phase A inclusions inside phase B matrix, or phase B

inclusions in a phase A matrix. It also doesn't provide the critical volume fraction f_c, which, for example, shows at which point a conductor becomes an insulator. According to this theory, a conductor remains a conductor until every element of it is replaced by an insulator. This is not realistic. There is also a third problem. This formula can apply to a system where inclusions of phase 1 are inside the matrix of phase 2, and they take up a volume fraction of f_1. It can also apply to a system where inclusions of phase 2 are inside a matrix of phase 1, and they take up a volume fraction of f_2. The formula doesn't yield the same result of ε_{eff} for both cases, when the systems can easily be considered identical. That is when $f_2 + f_1 = 1$.

The fourth problem with the Maxwell-Garnett theory is that it can't be easily generalized to more than two components.

2.3.2 The Bruggeman EMT

Another EMT is the Bruggeman approximation, published in 1935. It improves the Maxwell-Garnett relation in many ways. Like the Maxwell-Garnett EMT, it is derived by focusing on one particle and the local electric field that it is subjected to. This EMT was developed from the idea that the total polarization of the electric field is zero throughout the homogenized composite medium. Unlike the Maxwell-Garnett rule, it can be applied to more than just dilute composite media. It can be applied to an aggregate structure, where phase A and phase B are interdispersed and topologically equivalent [13]. It treats the two components symmetrically, so the third problem of the Maxwell-Garnett formula is avoided. It can even provide us with the critical threshold f_c. It is also easily expandable to multicomponent systems. It can apply to a system with i components, each taking up a volume fraction f_i and having a dielectric constant ε_i. The effective dielectric constant is expressed in the following equation:

$$\sum_i f_i \left(\frac{\varepsilon_i - \varepsilon_{eff}}{\varepsilon_i + 2\varepsilon_{eff}} \right) = 0$$

For a two-component system, the solution to this equation is

$$\varepsilon = \frac{1}{4} \left(\beta + \sqrt{\beta^2 + 8\varepsilon_1 \varepsilon_2} \right),$$

where $\beta = (3f_1 - 1)\varepsilon_1 + (3f_2 - 1)\varepsilon_2$. The critical point f_c can be predicted from this equation. It is possible to find out when an insulator-metal composite changes from a metal to an

insulator. In general, this equation is in agreement with experiments and computer simulations when $\varepsilon_1 \approx \varepsilon_2$, For the case $\varepsilon_1 >> \varepsilon_2$, the theory is in agreement with them only in two dimensions. That means the Bruggeman theory has a problem: the theory fails to predict effective dielectric constant in three dimensions, when $\varepsilon_1 >> \varepsilon_2$.

The Bruggeman theory can be improved upon using Green's functions, and the threshold value can be made independent of inclusion shape. Green's functions are a mathematical tool, useful for dealing with boundary value problems.

Bruggeman and Maxwell-Garnett formulas can also be used to find the effective thermal conductivity and effective electrical conductivity. For spherical inclusions, Bruggeman theory gives thermal and electrical conductivities:

$$\sum_i f_i \left(\frac{\kappa_i - \kappa_{eff}}{\kappa_i + 2\kappa_{eff}} \right) = 0$$

$$\sum_i f_i \left(\frac{\sigma_i - \sigma_{eff}}{\sigma_i + 2\sigma_{eff}} \right) = 0$$

There is also dynamic, or time-dependent effective medium theory. The time-independent EMT described above is relevant for composites whose disorder can be considered quenched, or fixed in place. Dynamic EMT is applicable to cases where particles move over time, as in colloidal suspensions, and cases where particles' properties fluctuate due to thermal and atmospheric fluctuations.

2.3.3 Applications

Traditionally, EMT was developed for electric and magnetic properties, and was useful for development of materials with specific properties of that nature. It could be materials such as high-voltage insulation, magnetic recording materials and capacitor materials. The EMT concept could also be applied to properties other than electromagnetic, such as elastic constants and viscosity.

2.3.4 Drawbacks

There are, unfortunately, problems that reduce the validity of most effective medium theories. The Maxwell-Garnett relation doesn't predict a threshold value. The Bruggeman EMT does, but its prediction of the critical value tends to be too large.

The critical threshold value the Bruggeman EMT predicts is closely connected with the shape of the inclusions. This violates the result of the percolation theory, which demands universality, or independence from inclusion shape. This theory is about formation of long-range connectivity in composite systems. The probability of a phase being connected in a giant long-range cluster has a finite percolation threshold concentration which is independent of the inclusion shape. If f_1 is below the percolation threshold, there is no long-range connectivity. If it is above, then there is long-range connectivity. The critical threshold f_c is expected to be identical to the percolation threshold, but EMT doesn't always predict that. However, it can predict the percolation threshold approximately.

To make matters worse, the percolation theory itself often doesn't give precise values for properties near the critical point. Critical transport exponents for percolation properties don't satisfy universality, and can vary from one continuum model to another. This adds another difficulty to the process of creating a good EMT.

EMTs presented so far are derived by focusing on one particle. They focus on the one-body problem, where the body is the single particle, surrounded by the effective medium. Extending it to a two-body or an *n*-body problem would make it a higher-order approximation.

Often, the EMT alone is not enough to explain results of experiments, and additional hypotheses need to be made. Sometimes, one of these hypotheses is the basic model used to describe the composite system. If empirical results don't match the predictions created by both the EMT and the basic model, either the model or the EMT could be blamed. It complicates the decision of whether an EMT is good or not. It is also worth noting that the properties of materials change as the material is reduced to nanoscale. Thermal transfer is different on the nanoscale, especially when grains are smaller than the mean free path of the phonons [ref21]. Both the Bruggeman and the Maxwell-Garnett EMTs say nothing about the size of the particles, and only consider the total volume fractions. It is up to the individual

researcher to find out how many phases with distinctive properties the sample contains, and which properties they have. A few real examples of such problems will be described in chapter 3.

Some sources state that the conventional effective medium theory is valid for effective transport properties when the inclusion size is larger than carrier mean free path and wavelength [17].

Chapter 3

Previous Research

A lot of research has been done to find good thermoelectric materials, and this chapter will sum up what has been done. The focus will be on nanostructuring as a means of increasing efficiency, and on the application of effective medium theories. Examples of effective medium theories will be discussed, and popular EMTs mentioned. The examples will show the effective medium theories in action. It will also be shown how determining the validity of an EMT is not straightforward, and depends on what basic model one uses to describe a specific system.

3.1 Finding effective thermoelectric materials

In 2011, the conversion efficiency of thermoelectric electricity generators ranged from 8 to 16.4% [11]. Research on finding efficient thermoelectrics tends to follow a simple formula: first, models are made, predicting how a specific structure, processing conditions, doping particle size and organization will affect the important properties. Then, the materials are synthesized. Their structure is characterized, and results of electric property measurements are compared to the models. So far, the main focus of the researchers has been on using low-dimensionality to reduce the thermal conductivity. However, it might not be enough to produce marketable thermoelectric devices. It is necessary to increase the power factor $\alpha^2\sigma$ and decrease the thermal conductivity κ at the same time. Fortunately, studies have shown that it's possible.

Latest research has found dramatic increases in the figure of merit by nanostructuring bulk materials, and thus lowering the lattice thermal conductivity. Nanostructuring can mean forming nanosized inclusions (nanodots, wires) of one phase inside a matrix of another phase. It can also mean creating a nanocomposite polycrystalline material, where all the grains are in the nanorange (ca. 5 nm – 10µm). A third type of nanostructured material is a thin-film superlattice [4]. This third type can be made by molecular beam epitaxy or chemical vapor deposition. It is in general a costly and difficult method, and this chapter will mostly focus on the other nanostructured thermoelectrics that were mentioned. It was also found, with both

models and calculations, and experimentally, that nanoparticles do not need to be organized into orderly arrays or layers to achieve reduced thermal conductivity [5].

There are two main ways to nanostructure an existing material in practice. One is based on forming the material from a melt, and making the nanoscale inhomogenities self-form by the processes of nucleation and growth, and phase segregation. This seems to be a good general way to make a thermoelectric material where nanoinclusions are encapsulated in a matrix phase, but there are rules to make it work:

1. The minority phase should be soluble in the matrix phase while in the liquid state, but not soluble in the matrix phase while it's solid.
2. The matrix phase should have an equal or higher melting point than the inclusion phase – the matrix phase will then solidify first and encapsulate the nanoinclusions.

It might also help to cause the melt to solidify rapidly, which would limit grain growth [18], although it might make the material less thermally stable at higher temperatures.

The second method of making nanostructured bulk is to grind up the existing single crystalline material into nanocrystals and then sinter them into a bulk sample [6]. This is a good general way to make a polycrystalline sample wholly made up of nanoscale grains.

An example of bulk materials where the matrix encapsulates nanoinclusions is the $AgPb_mSbTe_{2+m}$ family, or LAST-*m* (lead antimony silver telluride). It is, in turn, classified as a subgroup of PbTe- and PbSe-based materials. These are quenched from the melt or slowly cooled, and can spontaneously form nanostructures during the cooling process. When $m < 10$, slowly cooling the melt leads to phase segregation that is detectable by X-ray diffraction. There phases are larger microscopic areas, and don't help reduce the thermal conductivity [6]. However, when $m > 10$, the X-ray diffraction patterns imply a single phase, but investigation with TEM shows that the material is actually made of more than one phase. These nanoinclusions are on the nanoscale and reduce the thermal conductivity. To increase the material's power factor, it can be made n-type by introducing nonstoichiometry. $Ag_{1-x}Pb_{m+y}Sb_{1+z}Te_{2+m}$ has a *ZT* of 1.7 at ca. 700K. The LAST-*m* materials are predicted to be stable at temperatures below 900 K over long-term use. In fact, the material can be annealed at 870 K in a vacuum for months, and its electrical conductivity will increase, without degradation of any other useful properties.

Another material that has a high *ZT* is $Na_{0.95}Pb_{20}SbTe_{22}$ from the material family SALT-*m* (sodium antimony lead telluride). It also has a low thermal conductivity due to nanoinclusions. They are rich in Na and Sb. Its figure of merit is 1 at 475 K and 1.7 at 650 K [6].

In general, the PbTe-based nanocomposites showed reduction in thermal conductivity, when they contained nanoinclusions of phases such as Bi, Pb, Sb, SrTe and others [11]. Chalcogenide compounds were tested, as Bi_2Te_3 was for a long time known as the most efficient thermoelectric material near room temperature[13] . Nanostructured Bi_2Te_3 could even be used in a flat-panel solar thermoelectric generator, which achieved conversion efficiency of 4.6 – 5.4% [11].

As said previously, the nanoinclusions could also be wires, rather than dots. An example is the crystal pulled from the InSb-Sb eutectic alloy. The material contains rods of Sb in an InSb matrix. The thermal conductivity decreases with decreasing rod diameter.

To get an efficient “nanoinclusions in a matrix” thermoelectric, the matrix needs to be an already promising thermoelectric, while the inclusion phase must be capable of scattering phonons. For example, PbTe samples with <3% nanoparticles of Sb show reduced thermal conductivity compared to regular PbTe [6]. Some studies have shown that the host material can act as a barrier for grain growth of the inclusions, preserving the stability of the thermoelectric material. It is believed these nanoinclusions scatter acoustic phonons because of mass contrast between them and the matrix. Substitutions in alloys can also scatter phonons. They do it by introducing local lattice stress, due to difference in atomic mass and size [11].

An example of a nanocomposite polycrystalline material made up of nanograins is the p-type BiSbTe, prepared by ball-milling and hot-pressing. Its *ZT* values are 20% bigger at room temperature (1.2), and 40% bigger at 373 K (1.4) than those of the state-of-the-art ingot BiSbTe alloy [6].

Another material is the p-type boron-doped Si/Ge nanocomposite. It has a higher power factor than bulk SiGe alloys, due to enhanced Seebeck coefficient and despite the slightly lower electrical conductivity. The effect is due to the electron-filtering effects at the grain boundaries.

Half-Heusler alloys [11] is a group of bulk nanocomposites that can be good thermoelectrics. They have a general formula ABX, and they crystallize in the cubic structure. They have high thermal stability and they are abundant. Often, isoelectronic substitution at A-sites and B-sites is used to increase alloying scattering of phonons, and doping the X-site is used for carrier concentration modification. The p-type $Hf_{0.5}Zr_{0.5}CoSb_{0.8}Sn_{0.2}$ is a half-Heusler material with a *ZT* of 0.8 at 1000K. The n-type $Hf_{0.75}Zr_{0.25}NiSn_{0.99}Sb_{0.01}$ is also a half-Heusler, and its figure of merit is 1.0 at 600-700 °C. These can also be made with the simple method of high energy ball-milling the ingots, and dc-current assisted hot pressing of the nanopowder.

Skutterudites have also been improved by nanostructuring. They have the formula MX_3, where M is usually Co, Rh or Ir, and X is often P, As or Sb. They are relevant for thermoelectrics when heavy atoms are inserted into their icosahedral nanocages, often called "rattling atoms", because they generate local vibrations. These vibrations scatter phonons by introducing resonant states, as mentioned in chapter 2. The more cages are filled up with rattling atoms, the lower the κ_{latt} becomes. Some studies also show that there are local minima in κ_{latt} as a function of filler-to-host mass. Unfilled skutterudites can have useful *ZT* as well: nanoinclusion-containing $CoSb_{2.70}Te_{0.25}Sn_{0.05}$ has a *ZT* of 1.1 at 550°C [11].

There are a few other ways to make the nanoparticles that nanocomposites contain: wet-chemistry methods, molecular-beam epitaxy and inert-gas condensation methods [5].

Knowledge about scattering mechanisms is useful for optimizing thermoelectric performance of such nanosystems [5]. As previously said, scattering of charge carriers and phonons can increase the Seebeck coefficient and decrease the thermal conductivity, respectively. Studies have been conducted to find them. For example, new scattering mechanisms were found through property measurements in a PbTe-matrix material with embedded metallic Pb or Ag nanoparticles. Following temperature-dependent properties were found: carrier concentration (*n* or *p*), mobility μ, effective mass m^* and scattering parameter *r*. This last parameter is defined by carrier-scattering-relaxation parameter $\tau=\tau_0*E^{r-1/2}$. The value of *r* shows us what kind of scattering mechanism is observed. Metallic nanoinclusions in PbTe-matrix gave a scattering parameter greater than 3, a value no known scattering mechanism had at the time. It was concluded that the larger the *r*, the more energy-filtering effect there is, and the larger the gain in the Seebeck coefficient.

Making a polycrystalline material with nanoscale grains produces a lot more of grain interfaces than in materials with bigger grains. For example, the thermal conductivities of Si/ZrO_2 and the $Si_{0.8}Ge_{20}/ZrO_2$ composites were measured at 1000K. Both had ZrO_2 as the host material. The lattice thermal conductivity decreased as the inclusion dimensions decreased [12].

Some very interesting results were obtained for materials wholly made up of nanosized grains. Such a material is in the danger of grain growth, especially if it's designed for use at higher temperatures. Zhang *et al.* solved this problem for p-type $Bi_{0.4}Sb_{1.6}Te_3$ by adding some oleic acid into the materials before the ball milling process. This allowed them to reduce the grain size from 2-3 μm to 200-500 nm [11].

To make thermoelectrics an option capable of competing with less sustainable energy sources, they must also be cheap and made of abundant materials. PbTe-based thermoelectrics have high figures of merit, but they contain Te, which is rarer than Pt and Au in Earth's crust [11]. Magnesium silicides, especially $Mg_2Si_{1-x}Sn_x$ materials appear to be promising in that regard [19]. They are made of abundant materials and also don't have any toxic components. These have high carrier mobility. $Mg_2Si_{1-x}Sn_x$ has some fascinating band structure features, which allow density of states to rise without decreasing electron mobility. As a result, $Mg_2Si_{0.4}Sn_{0.6}$ has *ZT* of about 1.1 at a temperature between 700 K and 800 K, or an average *ZT* of 0.83 between temperatures 400 K and 850 K. $Mg_2Si_{0.6}Sn_{0.4}$ has a lower average *ZT* in the same interval (0.78), but it is more resilient under the effects of high temperature-induced oxidization and vaporization.

There is also another method, by which researchers attempted to make thermoelectrics cheap and efficient enough for mass-production. The idea is to combine inorganic semiconductor thermoelectrics and polymeric thermoelectrics into a nanocomposite [20]. Organic conducting polymers have some great features. They are cheap and easy to synthesize, have low density and low thermal conductivity. Unfortunately, mixtures of polymers and inorganic thermoelectrics tend to have low *ZT*, often less than 10^{-2} for room temperature. However, low cost might make them acceptably effective for use.

Examples of thin-film thermoelectrics are the Bi_2Te_3-Sb_2Te_3 thin films, the PbTe-PbSe thin films and thin films containing embedded quantum dots (figure 3.1). In these, phonon scattering can lead to minimal lattice thermal conductivities (0.2 – 0.5 W/mK) [4]. A B-

doped superlattice of PbSe quantum dot arrays, sandwiched between thin PbTe layers are reported to have *ZT* of 1.6 at 300K and 3.5 at ca. 570K [5]. This quantum-dot superlattice is said to have such high *ZT* values because of simultaneous increase in the power factor and decrease in thermal conductivity. *ZT* values higher than 2 have been reported for thin films, but it's hard to measure their properties, which makes the results difficult to reproduce [4]. In fact, in the first studies the thermal conductivities were not directly measured, but deduced from other measurements. Later measurements of κ gave much higher values, which cast doubt on the previous results [ref4]. Thin films also have another difficult problem: they are expensive to make, are not stable at high temperatures and are delicate. Therefore the researchers today choose to develop bulk nanostructured materials instead.

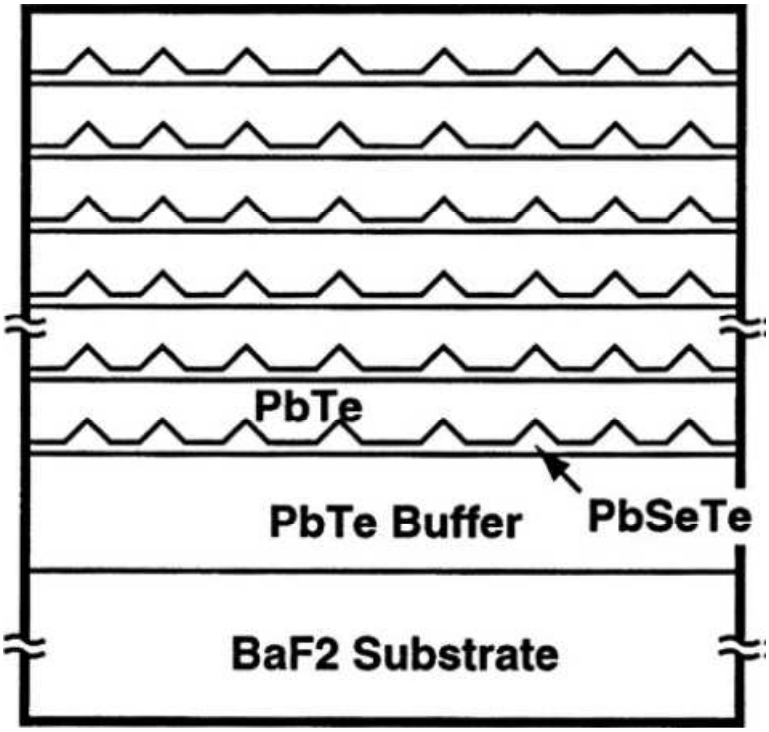

Figure 3.1: An example of a quantum-dot superlattice (QDSL). That main structure consists of PbSeTe as regular quantum dot arrays and PbTe as barriers. The structure is built up on BaF_2 substrate and PbTe buffer using Volmer-Weber island growth process [5].

In general, nanostructuring a material tends to increase the figure of merit, compared to a bulk material with the same composition. With embedded nanoinclusions, things are more complicated. If they are formed inside the host material through precipitation, they are likely to nucleate heterogeneously at grain boundaries and defects, which can in turn create an interconnected network of inclusion material [17]. This can lead to parallel conduction, which

is when heat and charge carriers don't move across boundaries between materials, but instead through each material. This, in turn, greatly diminishes the useful interfacial effects, such as energy filtering and phonon scattering. It is a hurdle to producing high *ZT* thermoelectrics through precipitation of inclusions.

3.2 Effective medium theory applied to thermoelectric materials

Effective medium theory has been applied to electrical conductivity, thermal conductivity and Seebeck coefficient of a material. It is already known that nanostructuring can increase the figure of merit. EMTs can provide quantitative analysis of how nanostructuring can increase the figure of merit. The Bruggeman approximation was successfully used to model the dielectric constant of many composite materials. For example, nanograins of PbTe, micrograins of PbTe, and air inclusions. Another composite material was made of nano-SiC, intergranular space, metallic inclusions and air.

Before moving onto descriptions of individual studies, the popular EMTs will be listed. They show up in many studies which use EMTs, although they are not the only ones.

C. W. Nan *et al.* created an EMT for effective thermal conductivity of a two-phase system. This EMT takes into account interfacial scattering of phonons, as well as thermal boundary resistance. The EMT was also prepared as an independent particle approximation. In the context of thermal conductivity, such an approximation assumes that no interparticle phonon scattering takes place. Because of that, it applies to systems with a small volume fraction of the inclusions. It is written as follows [12]:

$$\kappa = \kappa_{mat}\frac{\kappa_i(1+2\alpha)+2\kappa_{mat}+2f(\kappa_i(1-\alpha)-\kappa_{mat})}{\kappa_i(1+2\alpha)+2\kappa_{mat}-f(\kappa_i(1-\alpha)-\kappa_{mat})}$$

Here, κ_{mat} is the lattice thermal conductivity of the host material, κ_i is the lattice thermal conductivity of the inclusion material, f is the volume fraction of the particle inclusions and α is the thermal resistance parameter.

A second EMT that will be mentioned in the studies is the one made by J. J. Sonntag [13]. It is the Bruggeman formula, complemented with the Boltzmann transport equation for composite materials. The original formula was for thermal conductivity and Seebeck coefficient:

$$\sum_i f_i \frac{\frac{\kappa_i}{\alpha_i} - \frac{\kappa_{eff}}{\alpha_{eff}}}{\frac{\kappa_i}{\alpha_i} + 2\frac{\kappa_{eff}}{\alpha_{eff}}} = 0$$

Here, κ_{eff} and κ_i are effective thermal conductivity and the thermal conductivity of component *i*, while α_{eff} and α_i are the Seebeck coefficients. f_i is the volume fraction of the component *i*.

The third important EMT is the one devised by McLachlan *et al* [17]. It is also called GEM, the general effective medium theory. It applies to electrical conductivity σ, but can also apply to κ. It was developed by combining the percolation theory and the effective media theory [21]. The purpose of this EMT was originally for modeling electrical conduction properties of conductive inclusions inside polymer matrices. It is written as follows:

$$f_A \frac{\sigma_A^{1/t} - \sigma_{eff}^{1/t}}{\sigma_A^{1/t} + a\sigma_{eff}^{1/t}} = (1 - f_A) \frac{\sigma_{eff}^{1/t} - \sigma_B^{1/t}}{\sigma_B^{1/t} + a\sigma_{eff}^{1/t}}$$

Here, f_A is the volume fraction of component A, σ is an electrical conductivity, the constant $a = (1 - f_C)/f_C$. The value f_C is the percolation threshold, which is f_A at the point when precipitates of component A become interconnected. *t* is a critical exponent, related to aspect ratios and distributions of the inclusion phase. *t* often has to be fitted to the experimental data.

The fourth EMT was created by Bergman and Levy [17]. It can find the effective Seebeck coefficient α_{eff} based on thermal and electrical conductivities of a two-phase system. It often needs other EMTs to predict κ_{eff} and σ_{eff}, before it can be used.

$$\alpha_{eff} = \alpha_B + (\alpha_A - \alpha_B) \frac{\left(\frac{\kappa_{eff}}{\sigma_{eff}}\right)\left(\frac{\sigma_B}{\kappa_B}\right) - 1}{\left(\frac{\kappa_A}{\sigma_A}\right)\left(\frac{\sigma_B}{\kappa_B}\right) - 1}$$

3.2.1 Study 1 [12]

This first study picked the EMT by C. W. Nan *et al.* As stated earlier, it assumed no interparticle phonon scattering takes place. That isn't true for a composite with a high concentration of nanograins, and the EMT was modified by S. J. Poon and K. Limtragool. Their new version of the EMT accounted for interparticle scattering of phonons. It was created as a tool for screening for prospective high-ZT materials.

S. J. Poon and K. Limtragool modified the equation by increasing *f* infinitesimally to much higher than Nan's formula allows. It led to a differential form of $\kappa(f)$:

$$d\kappa = \frac{3\kappa\, df}{1-f}\left(\left(\frac{\kappa_i\left(1-\alpha(f)\right)-\kappa}{\kappa_i\left(1+2\alpha(f)\right)+2\kappa}\right) - \frac{3\kappa}{2C(f)v(f)\mathrm{a}}\right)$$

Here, $\alpha(f)$ is the thermal resistance parameter, or $\alpha(f) = \mathrm{R}(f)\kappa_{mat}(f)/(\mathrm{a}/2)$. R is the thermal boundary resistance and a is the particle dimension. $C(f)$ is the lattice specific heat and $v(f)$ is the average phonon velocity. This new resulting EMT is derived with the assumption that *f* should be able to be anywhere between 0 and 1. When $f = 1$, the inclusions fill the space completely. Spheres cannot do that, which is why the authors of the paper approximated the inclusions to be convex polyhedra. Therefore, the particle dimension "a" was defined as $\mathrm{V}^{1/3}$, where $\mathrm{V} = (\mathrm{a}^1\mathrm{a}^2\mathrm{a}^3)$, and a^1, a^2, a^3 are the sides of an orthorhombic polyhedron.

The validity of this EMT was tested by conducting experiments. First, monolithic nanocomposites were tested. These are materials were the lattice thermal conductivity of the inclusions is equal to κ_{mat}, and phonon mean free paths are the same in the matrix and the inclusion material. For these, the EMT by S. J. Poon and K. Limtragool is in good agreement with the experimental data, while the unchanged EMT by Nan overestimates the effective lattice thermal conductivity. It is a reasonable result, as the new EMT takes into account more of the phonon scattering events, which sink κ.

The EMT was also tested for two-phase non-monolithic nanostructured materials. Good agreement was found between calculated and experimental *ZT* and κ for several nanostructures alloys. Comparison with the same alloys pre-nanostructuring has shown that *ZT* can increase 30 – 130% due to nanostructuring alone.

This new EMT has a few drawbacks. The article mentions that while the new formula accounts for single and multiple-scattering processes, the multiple-scattering processes do not backtrack. Phonons scattered by the added particles are not rescattered by the preexisted particles. Thus, this formula accounts for only a fraction of all the multiple-scattering events. In general, the fraction of r-th order scattering processes represented is $f \approx 1/r!$. The second problem is that lattice specific heat $C(f)$ and average phonon velocity $v(f)$ are dependent on the phonon frequency ω, and rigorous computations that require knowledge of phonon dispersions are needed to solve the equation and find κ.

3.2.2 Study 2

T. Kyratsi, E. Hatzikraniotis, M. Ioannou, D. Y. Chung and I. Tsiaoussis used the effective medium theory in their own study of the amorphous/crystalline β-$K_2Bi_8Se_{13}$ nanocomposite [13]. Their material was created by ball-milling and cold-pressing into pellets. The EMT they used was a modification of the one devised by J. J. Sonntag.

This formula did not initially match with the experimental data of T. Kyratsi *et al.*. The components initially taken into account were the crystalline phase, the amorphous, and the air inclusions. Later, the crystalline phase was divided into nanocrystallites and microcrystallites. It is known that nanosizing a material leads to change in its properties. This switch from a three-component to a four-component system lead to a much better fit between hypothesis and experiment, as shown in figure 3.2 [13]. Here, $f_{m\text{-}CR}$ is the volume fraction of microcrystallites, $f_{n\text{-}CR}$ is the volume fraction of the nanocrystallites, f_{AM} is that of the amorphous phase, and f_{AIR} is that of air inclusions or pores. The dotted lines show the three-component predictions, while the solid line is the four-component prediction. The spheres are the experimental data.

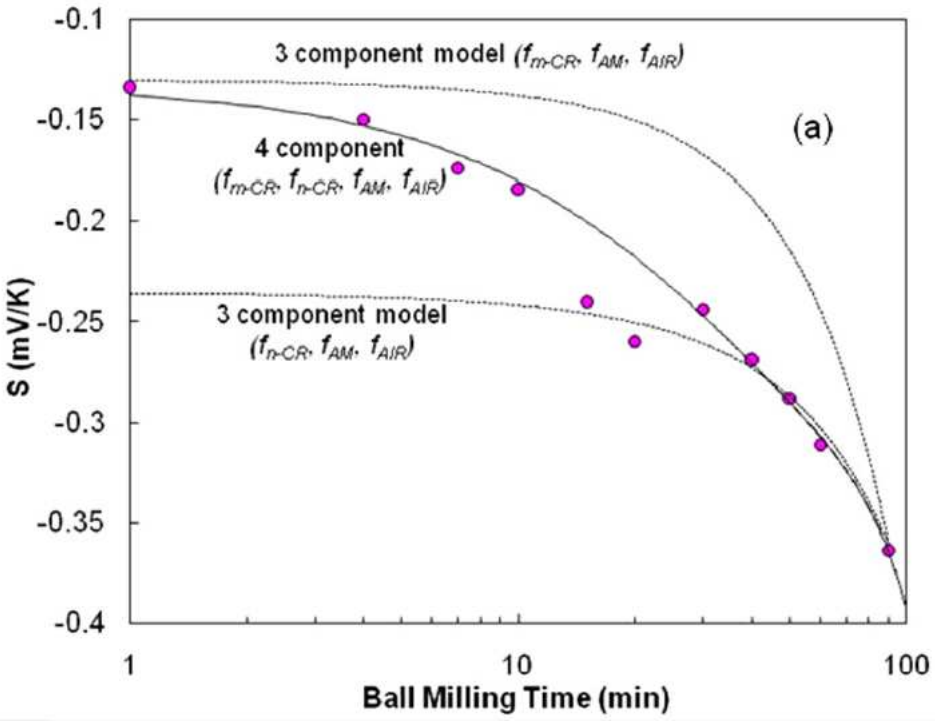

Figure 3.2: Experimentally determined Seebeck coefficient (spheres) and theoretical Seebeck coefficient (lines), vs ball milling time.

This study shows how choice of phases in the model changes if an EMT appears valid or not.

3.2.3 Study 3

P.A. Sharma, J. D. Sugar, and D. L. Medlin studied Sb_2Te_3 nanoinclusions in an $AgSbTe_2$ matrix [17]. The Sb_2Te_3 inclusions formed interconnected networks by precipitating preferentially at the grain boundaries and defects of the matrix. According to the effective medium theory, *ZT* of a composite can't become larger than that of its components, if the interface effects are neglected. If the heat and charge currents are allowed to move without crossing grain boundaries, as happens in the case of interconnected network of the phases, then nanostructuring can actually decrease *ZT*. One EMT used in this study was proposed by McLachlan *et al.*, and the other one by Bergman and Levy. Electrical and thermal conductivities of the material were found though the first EMT, while the latter was used for finding the Seebeck coefficient.

The volume fractions of the matrix and the inclusions were estimated by determining precipitate area fraction, using optical micrographs. The EMT used fitted with the measured data. This study showed that morphology of the inclusions can play a major role in the effective transport properties. Because the inclusions precipitated at the grain boundaries and planar defects, they formed an interconnected network, and suppressed the beneficial interfacial effects, thus lowering *ZT*.

3.2.4 Study 4 [22]

One study, conducted by G. Hurvits *et al.*, focused on composite films of Al and Ge. These were 2000Å films deposited on glass slides. In this study, the EMT by Bergman and Levy was tested. It describes a two-component system. In this case, phase M is the metallic phase, aluminium. Phase I is the insulating phase, which is amorphous Al-doped germanium. Then the EMT looks like the following equation:

$$\alpha_{eff} = \alpha_M + (\alpha_I - \alpha_M)\frac{\left(\frac{\kappa_{eff}}{\sigma_{eff}}\right)\left(\frac{\sigma_M}{\kappa_M}\right) - 1}{\left(\frac{\kappa_I}{\sigma_I}\right)\left(\frac{\sigma_M}{\kappa_M}\right) - 1}$$

To test the validity of this theory, the researchers used another two EMTs to find the thermal conductivity κ_{eff} of their samples, as data was not available. The first one is a modified Bruggeman asymmetric EMT, devised by Every *et al.*, and is

$$(1 - f_M)^3 = \left[\frac{\kappa_I}{\kappa_{eff}}\right]^{(1+2a)/(1-a)} \left[\frac{\kappa_{eff} - \kappa_M(1-a)}{\kappa_I - \kappa_M(1-a)}\right]^{3/(1-a)}$$

Here, f_M is the metallic volume fraction, a = a_K/a, a is the radius of the dispersed metallic particles, a_K is the Kapitza radius. a_K is defined as $a_K = R_{bd}\kappa_I$, where R_{bd} is the boundary resistance at the interface between the phases. It can be written as a ratio between heat flux and the temperature discontinuity across the interface.

The second EMT used was the GEM equation, created by McLachlan. It is somewhat rewritten in this study:

$$\frac{(1 - f_M)(\sigma_I^{\frac{1}{t}} - \sigma_{eff}^{\frac{1}{t}})}{(\sigma_I^{\frac{1}{t}} + A\sigma_{eff}^{\frac{1}{t}})} + \frac{f_M(\sigma_M^{\frac{1}{t}} - \sigma_{eff}^{\frac{1}{t}})}{(\sigma_M^{\frac{1}{t}} + A\sigma_{eff}^{\frac{1}{t}})} = 0$$

Electrical resistivity and Seebeck coefficient were measured experimentally. Experimentally measured σ values, and κ values calculated with the last two EMTs were inserted into the EMT created by Bergman and Levy. This resulted in two predictive $\alpha(f_M)$ graphs. They were compared to experimental α values. A good fit was achieved, as seen in figure 3.3.

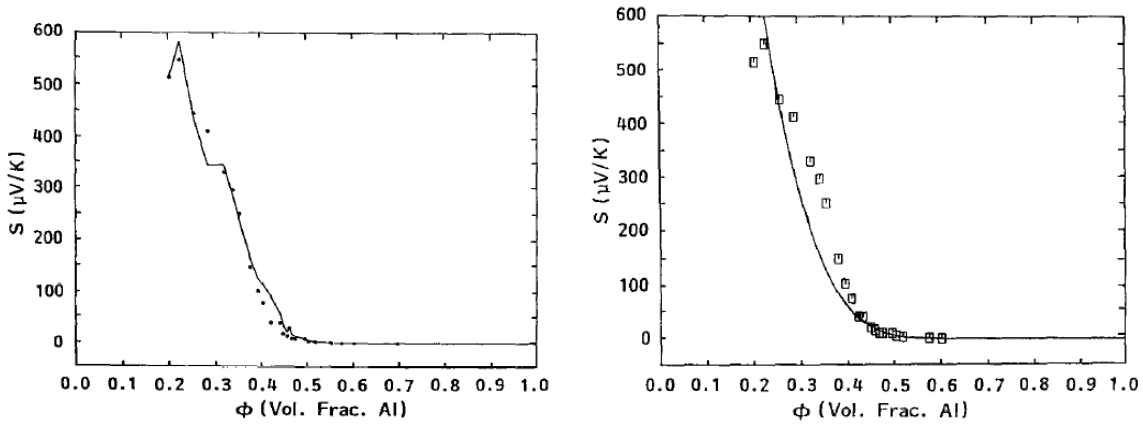

Figure 3.3: Experimental and theoretical Seebeck coefficient (here, S (μV/K)), vs. volume fraction of Al (here, ϕ). Dots are the experimental values, while solid lines are the theoretical curves. Left: curve made using the Bergman-Levy EMT and the Every EMT. Right: curve made using the Bergman-Levy EMT and the GEM equation.

3.2.5 Study 5

Thomas Stöker, Anne Köhler and Ralf Moos conducted a study on a PEDOT (poly(3,4-ethylenedioxythiphen)) and PSS (poly(4-styrene-sulfonate) conducting composite [21]. Earlier, it was found that in terms of EMT, the PEDOT/PSS composite is better described as a PEDOT-PSS/PSS composite. PEDOT-PSS complexes are highly conductive, while the PSS matrix is not. The GEM equation was used to describe how σ changes when the PSS content increases. The electrical conductivity decreased with increasing PSS content, until this component dominated the property. PEDOT:PSS ratio lower than 1:6 causes the decrease in σ to slow down rapidly and then stop. This result reflects that electrical conductivity of this material has a critical percolation ratio. On one side of this ratio, conduction is dominated by the ionic PSS electrolyte. On the other side of this ratio, it is dominated by the adjacent highly conductive PEDOT-PSS particles. Figure 3.4 shows the measured σ and the theoretical σ calculated with the GEM equation. The percolation fraction of the highly conductive inclusions is shown in the figure as ϕ_c. Theory and data seems to achieve a relatively good fit. However, this material has a very low *ZT*, and is therefore only useful for energy harvesting where only low power densities are needed, while the thermoelectric device is required to be bendable.

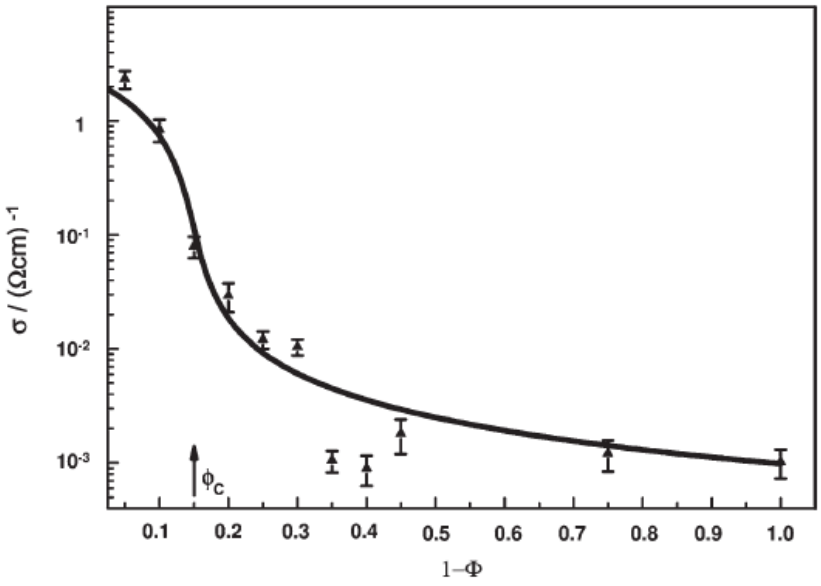

Figure 3.4:Experimental (symbols) and theorerical (line) electrical conductivity σ of the PEDOT/PSS composite, vs. normalized PSS content 1-ϕ (relative to PSS_{max} = 20). The percolation fraction of the conducting inclusions is ϕ_c.

3.2.6 Study 6 [23].

This study by F. Hao, D. Fang and Z. Xu investigated thermal conductivity of aligned Ge nanowires inside a crystalline Si matrix. Here, an EMT was applied not only to the two most obvious phases, but also to a third one. It is called the thermal boundary phase (TBP). Half of this phase is germanium, and another half is silicon. As implied, it is the area that consists of the Si/Ge interfaces, and their immediate surroundings. This phase originates from the mismatch of group velocities of phonons, v_g, on different sides of the interface. This mismatch leads to strong phonon scattering. The thermal conductivity of this phase is obtained from molecular dynamics simulations.

The EMT used to predict the effective κ was the modified EMT (MEMT), devised by Nan *et al.* Since the material is likely anisotropic, two thermal conductivities were predicted: transverse κ (κ_T) perpendicular to the Ge wires, and longitudinal κ (κ_L) along the wires:

$$\kappa_L = (1 - f)\kappa_{mat} + f\kappa_i$$

$$\kappa_T = \kappa_{mat}\frac{\kappa_i(1+\mathrm{a}) + \kappa_{mat} + f(\kappa_i(1-\mathrm{a}) - \kappa_{mat})}{\kappa_i(1+\mathrm{a}) + \kappa_{mat} - f(\kappa_i(1-\mathrm{a}) - \kappa_{mat})}$$

In these equations, f is the volume fraction of Ge nanowires, and a = $R_{K*}\kappa_{mat}/a$, where $R_{K*}\kappa_{mat}$ is the Kapitza radius, and a is related to the cross-section of the wire. F. Hao *et al.* also used the classical EMT:

$$\kappa_L = f_{Si}\kappa_{Si} + f_{Ge}\kappa_{Ge} + f_{TBP}\kappa_{TBP}$$

$$\frac{1}{\kappa_T} = \frac{f_{Si}}{\kappa_{Si}} + \frac{f_{Ge}}{\kappa_{Ge}} + \frac{f_{TBP}}{\kappa_{TBP}}$$

Both models were compared to experimental results, as shown in figure 3.5.

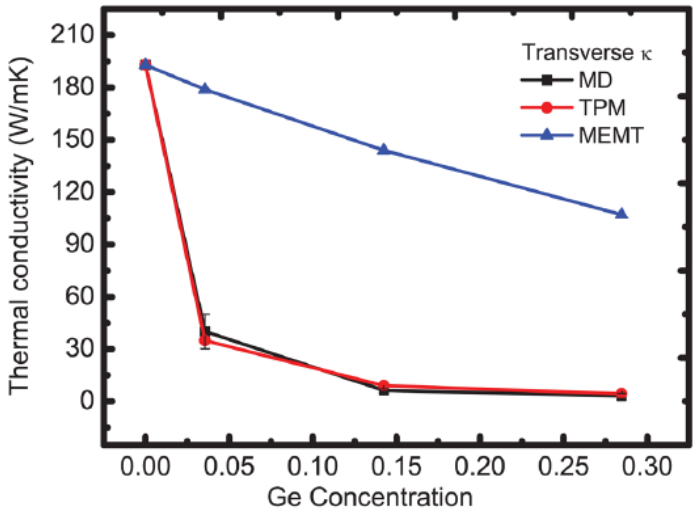

Figure 3.5: Experimental (MD) and theoretical (MEMT, TPM) thermal conductivity of a Si/Ge composite, vs. Ge concentration.

κ_T is best predicted by the second model, while MEMT is not even close to a good fit. While both EMTs take the interface effects, MEMT considers the interface thickness to be infinitesimal. This assumption fails when the material is nanostructured, and the interface thickness is comparable to the inclusion size.

κ_L is not predicted well by either of the models. They overestimate it. It could be because the materials are in the nanoscale, and phonon mean free paths are much smaller than in bulk materials. Mean free paths are related to the κ in the following manner:

$$\kappa = \sum_i C_i v_i^2 \tau_i$$

The sum is over all phonon modes i. C_i is a specific heat, v_i is a phonon group velocity, and τ_i is a phonon lifetime. Mean free path of a phonon is $l = v\tau$. It is likely that lattice mismatch at the boundaries partially causes the failure of both theories. To improve the EMT, κ of each phase needs to be substituted with the effective κ that contains these effects.

3.3 Previous measurements of thermoelectric properties of silicon

Silicon is an important material within the field of semiconductor technologies. The material is easy to handle and its electronic, thermal and mechanical properties are relatively easy to vary according to need.

As shown by many studies that used EMT, porous polycrystalline material can be thought of as a composite system. The first phase involved is the silicon crystals. The second phase is the atmosphere found within the channels, or closed and open pores that formed during sintering.

Some studies were conducted to find dependence of thermoelectric properties on porosity. It was found that changing the density by just a few percent can change the electrical conductivity by orders of magnitude. Therefore, achieving close to theoretical value for density during sintering appears to be very important. At the same time, higher porosity leads to lower thermal conductivity. It is especially true when nanoscale pores are present [13]. Some reports show that nanoporous silicon has a κ two orders of magnitude smaller than that of bulk silicon [23]. It occurs because of strong scattering of phonons at the interface, and depression of the long-wavelength phonons.

Chapter 4

The General Experimental Methods

This chapter will describe the experimental methods that will be used in this thesis work. The principles behind the methods will be explained. Each subchapter also contains the advantages and the limitations of each method.

4.1 Preparation of single crystal silicon samples

Six boron-doped silicon wafers were purchased. The plan requires comparison between the thermoelectric properties of single-crystalline and polycrystalline silicon. The instruments that measure these properties only accept specific sample sizes and shapes. Thermal conductivity instrument has the most inflexible requirements. Its sample holders are fit for 8mm x 8mm square samples, 10mm x 10mm square samples, and for circular samples with a diameter of 12.7mm. To create single-crystalline samples of silicon, the wafers are simply cut with a hard, sharp diamond pen parallel to the crystallographic planes. It is enough to create a small scratch. The crack it creates will propagate easily through the thickness of the wafer when some force is applied to break it. It happens because the crystal is weaker between crystallographic planes. It is recommended to handle the single-crystalline silicon bits with tweezers and not one's fingers – this protects the silicon bits from contamination. One can also use gloves. If the sample is slightly bigger than 10mm x 10mm or 8mm x 8mm, then it can be temporarily glued to a rod with those exact dimensions, and its extending edges can be polished away.

4.2 Synthesis of polycrystalline silicon

A polycrystalline sample can be made by crushing, ball-milling a single-crystalline wafer, and then sintering the powder under pressure and elevated temperature. Crushing isn't likely to produce powders with a constant grain size, and so ball milling is necessary. The result of ball-milling is a fine powder. It is best to use a mortar and a pestle of agate (SiO_2) for crushing, and a cup and balls of the same material for ball-milling. This minimizes contamination of silicon.

To prepare the powder for sintering, it's cold-pressed into a small cylinder. This cylinder is then placed inside a sintering machine, where it's heated up and subjected to pressure over many hours. Together, the grains of the powder have a large surface area, and a large surface energy. For elemental solids, minimization of the surface free energy is the driving force of the sintering process [24]. Grains connect to each other and in the end of the process, we have a solid, dense, polycrystalline material. This method, when used to prepare nanocomposite polycrystalline materials, has some limitations. To achieve good thermoelectric properties (such as high carrier mobility), total removal of the oxide layers is necessary. Whenever organic binder is used under cold-pressing of the powder, its removal is also necessary. It is also challenging to obtain highly dense samples [6]. Sintering also has a disadvantage compared to simply cooling a material from the melt – it produces incoherent, rough interfaces between the grains, which scatter electrons more than coherent, epitaxy-like interfaces. Despite these drawbacks, the technique has some advantages. Powder technology has low cost, it can be used for mass production, the material can be shaped into specific shapes, and anisotropy is eliminated [13]. Along with techniques based on spinoidal decomposition and precipitation, it is much easier and less costly than epitaxial growth and thin-film deposition techniques.

If the sintering machine is not available right after cold-pressing the powder into a cylinder, it's necessary to somehow shield that cylinder from oxygen. It is still made of silicon powder that is loosely held together. Therefore, it has high surface area, and will easily be oxidized, forming a lot of SiO_2. A way to protect the silicon powder from oxygen and store it safely overnight is to use an atmosphere of the inert argon gas. Glove bags are made just for that purpose. One can pump the oxygen out of the glove bag and fill it with argon. Then one can handle the objects inside the glove bag, which includes the fine silicon powder, and it will be safe from oxygen's unwanted influence. Inside the bag, the powder can be transferred into a cold-press. The cold-press can be taken out of the bag and quickly used to compress the powder into a cylinder, which is then quickly put inside a desiccator. The desiccator, in turn, will keep the sample in a vacuum.

After sintering, the solid polycrystalline sample could be cut and polished into the desired shape.

4.3 Density and porosity determination of the polycrystalline silicon sample

Once a sintered polycrystalline sample is made, its porosity needs to be measured. To measure the empty space or air content of the polycrystalline material, two methods can be employed.

4.3.1 The geometric method of porosity determination

One method of porosity determination is the simple geometrical method. The dimensions of the sample are measured, and the volume V is calculated. The mass m of the sample is also measured. The density of the sample is found through the equation $\rho = m/V$. Then one can look up the density of the single crystal silicon, ρ_{Si}. The volume of empty space in the sample is then

$$V_{pores} = V - \frac{m}{\rho_{Si}}$$

And porosity is defined in the following equation:

$$Porosity = \frac{V_{pores}}{V_{solid} + V_{pores}}$$

Here, V_{solid} is the volume of the solid only, while V_{pores} is the volume of the pores in the sample. Together, these two values are equal the measured volume of the sample, V. This is a very simple, but useful method. However, the accuracy of this method is limited, if the sample has uneven surfaces or geometry. It is also problematic if materials other than silicon are present. They will have a different density. If enough is present, such a material will affect the accuracy of the calculations.

4.3.2 The Archimedes method for porosity determination

The second method for measuring porosity is the gravimetric method, or the Archimedes method [25]. It has better accuracy, if specific assumptions are obeyed. It is based on the Archimedes's principle: when a body is partially or totally immersed in fluid, the fluid exerts an upwards force on the body, which is equal to the weight of the fluid that is displaced by the body.

The sample is first weighed in air, which gives the value M_{air}. This value can also be expressed in the equation $M_{air} = V_{air} \cdot \rho_{Si}$, where V_{air} is the volume taken up by the solid

material (expressed as V_{solid} in subchapter 4.3.1), and ρ_{Si} is the mass density of single-crystalline material, in this case silicon. Then the sample is hung on a string and weighed while fully submerged in water, yielding a value M_{water}. It means the downwards force on the string is $F = M_{water} \cdot g$. It is also subjected to two more forces: the upward buoyant force, equal to the weight of displaced water ($m_w \cdot g$), and gravity ($M_{air} \cdot g$). Figure 4.1 helps visualize all the forces. Since the sample doesn't move, the sum of vertical forces is zero. This fact leads to the following equation: $M_{air} \cdot g = m_w \cdot g + M_{water} \cdot g$. It is assumed that the water doesn't penetrate into the pores, because they are small. Thus, m_w is equal to $(V_{air} + V_{pores}) \cdot \rho_w$, where ρ_w is the mass density of water.

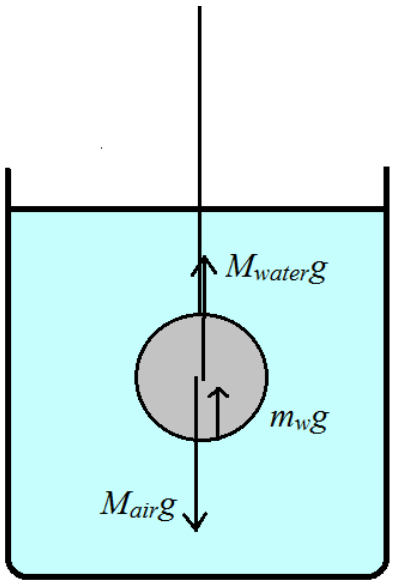

Figure 4.1: A schematic representation of the forces acting on the porous sample, when it is weighed in water. The sample is hung on a string, and submerged in a glass of water. Forces are drawn as arrows.

Porosity is defined as it was defined for the geometric method. From all the equations already mentioned in the previous paragraph, it is possible to calculate this value:

$$Porosity = 1 - \frac{M_{air}\rho_w}{(M_{air} - M_{water})\rho_{Si}}$$

4.4 Microstructure characterization of the polycrystalline Si sample

The microstructure of the polycrystalline sample will be analyzed using the optical microscope, the TEM and the SEM.

4.4.1 Optical microscopy [26]

Reflection optical microscopy is the relevant type, when the sample is metallic or semiconducting. Samples that contain conduction electrons are opaque to visible light. In such samples, contrast stems from surface topology, or due to difference in absorption of visible light. Difference in light absorption is what makes the material have color. Viewing the sample under the optical microscope can sometimes reveal if the sample has several phases, and if it contains bigger grains. Techniques using polarized light create contrast due to the difference in orientations of crystalline phases, and can reveal if there is any amorphous glass phases. It can't detect an amorphous thin layer of glass at the surface of a silicon sample, however, but this layer is expected to form due to interactions with oxygen. Dark-field images can help view topological details that aren't readily discernible in the bright-field setting.

4.4.2 TEM [26]

A TEM is a microscope that uses electrons instead of visible light waves, and electromagnetic lenses instead of optical glass lenses. The thin slice of the sample is irradiated with a beam of high energy (100-400 keV) electrons. They can be generated by applying a high acceleration voltage to a heated filament. Most of these electrons go right through a sample. The rest of the electrons are scattered in various ways, and generate secondary signals in the sample. Forward scattered electrons are used to obtain images and diffraction patterns of the sample. These electrons exit the sample and impinge on a fluorescent screen, which is visible to the viewer. Images are useful for studying the sample's microstructure and defects. A diffraction pattern can tell us about the crystallographic characteristics of the specimen and orientation of the specimen relative to the electron beam. A TEM also has the added function of chemical analysis: EDS (energy-dispersive spectrometer) and EELS (electron-energy loss spectrometry).

The function of the TEM that is relevant in this thesis is imaging. It is useful to find grain size and pore size in the sample. A TEM sample needs to be very thin, or else the beam will not go through it, and no useful image or diffraction pattern will be obtained. The images created by TEM of thin samples show no depth sensitivity. A TEM image gives us a picture of the surface, the bottom of the sample, and everything between them. It is a two-dimensional image. Because of this, finding pore size with TEM might be hard. However, TEM is perfect for finding grain size. Using bright field of dark field imaging can create contrast due to

orientation of individual grains. Dark field imaging picks one diffraction spot, and uses it to create the image. Only grains with the correct crystallographic orientation will appear bright in the image. A bright field image picks only the central diffraction spot, which excludes the strongly scattered electrons.

A thin sample must be prepared for TEM analysis. Since the sample is porous, simply thinning out a sample won't work. It is likely to fall apart. Another route can be used: first, a relatively thin portion of the material will be filled with glue through its pores, and then the sample will be thinned out. For thinning out, polishing paper with small particle sizes can be used. The last stage of thinning out can be done by using an ion milling instrument. It accelerates atomic ions and sends them at the center of the thin sample. If the ion beams have a low incident angle (for example, 5°), then the material will be removed slowly, without inducing too much damage. It will also form a wide, shallow hole through the sample, rather than a steep deep one.

4.4.3 SEM [26]

SEM, unlike TEM, can't aid in finding grain size, but it can instead aid in finding pore size. The method allows the researcher to obtain images of the surface topography.

A SEM scans a focused electron beam across the sample in a raster pattern. Beam energies are around 3-30 keV. Samples can be thick, and much bigger than samples required for TEM. The electron beam hits the surface, and generates a variety of response signals, which originate in a small volume near the surface. The response signals are collected by detectors surrounding the sample and amplified. Then the signal is displayed on a monitor. It creates a three-dimensional image of the surface with depth-sensitivity. Some of the signals coming from the sample can be used for EDS, like in TEM. However, since the signal comes from a larger volume of material than in TEM, this EDS doesn't have as good resolution.

To prepare the sample for SEM analysis, it is usually covered with a thin layer of conducting material – carbon. It stops the electrons from building up on insulating samples.

4.5 Electric characterization of the Si samples

The following properties are to be measured on both the polycrystalline and the single crystalline samples: effective resistivity, effective Hall mobility, carrier concentration,

Seebeck coefficient and thermal conductivity. All will be measured in the temperature range between 77 K and 650°C, if possible.

Three different setups will be necessary to measure all these properties. One setup is for thermal conductivity, another is for the Seebeck coefficient, and the third one is for everything else.

After the measurements, these properties are displayed as graphs, where temperature is the x-axis. A computer program is used to plot them.

4.5.1 Resistivity, Hall mobility and carrier concentration

The Hall effect can be used to obtain resistivity, Hall mobility and carrier concentration measurements at the same time. This subchapter will first describe the Hall effect. Then it will describe in simple terms what is measured during this experimental method, and how the needed properties are calculated. Then the subchapter will briefly describe the practical setup for the measurements, and describe the calculations specific for that setup. At the end, advantages and disadvantages of this method will be discussed.

The Hall effect is observable when a conducting sample is placed in a uniform magnetic field that is perpendicular to the current direction. The electric field E_x is causing the charge carriers to move in the x-direction. The moving charge carriers are deflected by the magnetic field with a force $\boldsymbol{F} = q\boldsymbol{v} \times \boldsymbol{B_z}$, and collect at one side of the sample. This leads to a buildup of charge on one side, which creates an electric field E_y, which is perpendicular to both the current direction and the magnetic field.

The general expression for resistivity is

$$\rho = \frac{E_x}{J_x},$$

where J_x is the current density. Resistivity can thus be measured without applying a magnetic field. The Hall coefficient, however, depends on it, and is expressed with the following equation:

$$R_H = \frac{E_y}{J_x B_z},$$

where B_z is the magnitude of the applied magnetic field. However, electric fields and current densities can't be measured directly. Instead, one measures currents and voltages between different contacts on the sample. Thus, resistivity and the Hall coefficient can be found. Finding ρ and R_H aids in finding carrier concentration and mobility.

Hall theory states that for low magnetic fields, the Hall coefficient R_H is written as:

$$R_H = \frac{r(p-b^2n)}{q(p+bn)^2}$$

Here, r is a scattering factor, lying somewhere between 1 and 2, but usually assumed to be 1. $b = \mu_n/\mu_p$, a ratio between electron and hole mobilities, and p and n are hole and electron concentrations, respectively. This equation works when $B<<1/\mu_n$ for $p>>n$, or when $B<<1/\mu_p$ for $p<<n$.

Experimentally, R_H is found through this equation:

$$R_H = \frac{tf(V_1^H, V_2^H, \ldots \ldots V_8^H)}{B_z I}$$

Here, t is the sample thickness, a V^H is a the Hall voltage, $f(V^H_1, V^H_2, \ldots \ldots V^H_8)$ is a specific function of all the measured Hall voltages which will be described in the next few paragraphs. B_z is the magnetic field, and I is the current. Resistivity similarly depends on the measured voltages and the current. With the combination of these two equations, p or n could be calculated.

The mobility can be found from the Hall coefficient and the resistivity. There are actually several carrier mobilities described in literature, and in it is the Hall mobility that is measured in this master thesis work. It is defined with the following equation:

$$\mu_H = \frac{|R_H|}{\rho}$$

The instrument suitable for all these measurements uses the four-contact probe arrangement, or the Kelvin technique [27]. A sample is connected to four electrodes, either by simply pressing them onto the sample, or by soldering them onto the sample. Two electrodes measure voltage, while the other two supply current.

There are two variations of the Kelvin technique: the four-point collinear probe method and the van der Pauw method. The latter is the relevant one for this thesis, but the four-point collinear probe method deserves a short explanation. During the four-point collinear probe method, the four electrodes are placed along the same line, which goes through the center of the material. The probe spacing is equal between each probe.

In the van der Pauw arrangement, contacts are used instead of electrodes. The four contacts are soldered to the sample's circumference. The sample is often either square or circular. In theory, a flat sample of any shape can be used, as long as four conditions are met:

1. The contacts are attached at the circumference of the sample.
2. Contacts are sufficiently small.
3. The thickness of the sample is uniform.
4. The sample is singly connected, meaning it contains no isolated holes.

When the van der Pauw arrangement is used, it gives rise to specific equations, which can be used to find resistivity, Hall mobility and carrier concentration. The resistivity is calculated using the following equations:

$$\rho_A = \frac{\pi t}{\ln(2)} f_A \left[\frac{V_1 - V_2 + V_3 - V_4}{4I}\right]$$

$$\rho_A = \frac{\pi t}{\ln(2)} f_B \left[\frac{V_5 - V_6 + V_7 - V_8}{4I}\right]$$

$$\rho_{AVG} = \frac{\rho_A + \rho_B}{2}$$

Here, ρ_{AVG} is the average resistivity. f_A and f_B are geometrical factors, also found through measured voltages. [27]. So, eight measurements of voltage are needed to find resistivity at each current and temperature. They are shown in figure 4.2:

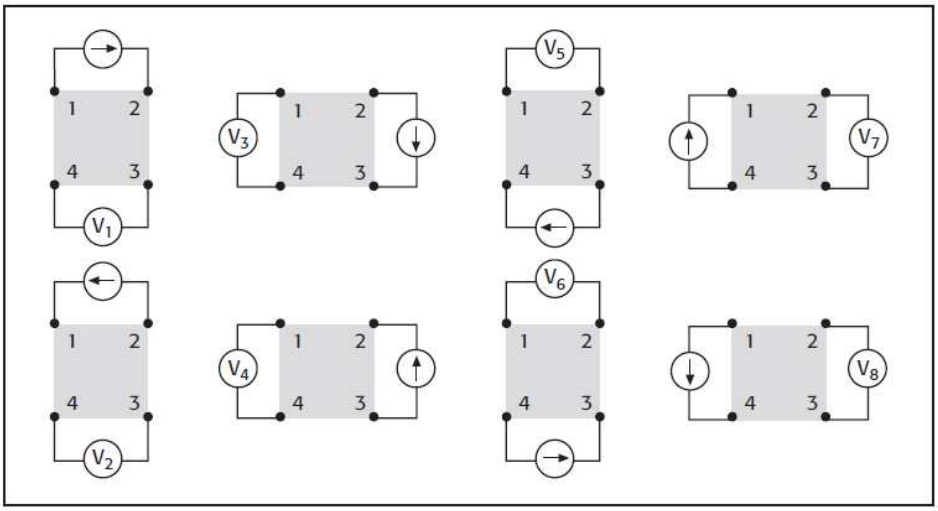

Figure 4.2: The voltage measurements necessary for calculation of the resistivity of the sample in the van der Pauw arrangement [27].

Hall mobility, carrier type and concentration can also be derived from measuring voltages and currents. However, this time the configurations are different, as seen in figure 4.3. The Hall voltage is measured in those configurations. Then the direction of the current is reversed, and voltages are measured again. Then the direction of the magnetic field is reversed, without changing its magnitude. Four more Hall voltages are measured as previously. This way, eight voltages are measured, which will be called V_{H1}, V_{H2}, … …V_{H8}.

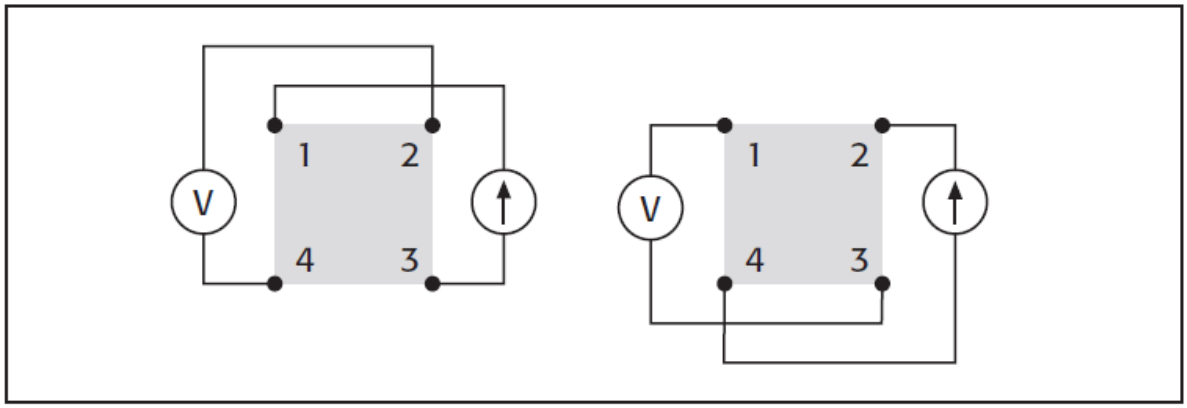

Figure 4.3: Two of the voltage measurements necessary for calculation of the Hall coefficient in the van der Pauw arrangement [27]

Two Hall coefficients are then found:

$$R_{HC} = \frac{t\, f(V_{H1},V_{H2},V_{H3},V_{H4})}{B_z\, I}$$

$$R_{HD} = \frac{t\, f(V_{H5},V_{H6},V_{H7},V_{H8})}{B_z\, I}$$

Here, B_z is the magnetic field, t is the thickness, $f(V_{H1},\ldots\ \ldots V_{H4})$ is a function of those measured voltages, and I is the current. Average Hall coefficient is:

$$R_{H\text{-}AVG} = \frac{(R_{HC} + R_{HD})}{2}$$

And Hall mobility is $\mu = |R_{H\text{-}AVG}|/\rho_{AVG}$.

Often, the instrument allows the temperature to be changed. Then one can make $\rho(T)$, $\mu(T)$ and $p(T)$ (or $n(T)$) graphs.

Using four contacts instead of two has major advantages. If only two electrodes are used, voltage is measured not only over the semiconducting sample itself, but also over a portion of the current-carrying wire, and the current-carrying contacts that connect electrodes to the sample. Two-point probe method depends on a lot of calibration. Using four electrodes eliminates measurement errors due to probe resistance (resistance of the current-carrying wire), spreading resistance under each electrode and contact resistance between each metal probe and the semiconducting specimen [28].

Using the van der Pauw arrangement specifically has advantages, too. The contacts or electrodes take less space than four collinear electrodes, which allows samples to be smaller. Van der Pauw arrangement also eliminates the need to measure sample widths and distances between the contacts. There are also some disadvantages. One disadvantage is that the finite contact size introduces errors into the measurements [29].

The main topic of this subchapter - the Hall method - has several advantages. One is that it provides average values of carrier concentration and carrier mobility for non-uniformly doped samples. This method also has some disadvantages. One source of error in resistivity measurements is carrier injection, from the metal-semiconductor contacts. This effect is non-negligible at high currents and leads to enhanced conductivity readings. The second source of error is pressure-induced band gap narrowing, which in turn enhances the carrier injection effect. [28]. It could happen if metal electrodes are pressed against the semiconductor sample.

The third error source is due to temperature gradients. These can happen at high currents, which will heat up the sample in a non-uniform manner, and produce thermoelectric voltages. Uneven temperature can also come from fluctuations of temperature in the room. And last, but not least, this method is slightly damaging. Due to contact with the electrodes, it can deform the surface or deposit some metal on it.

4.5.2 Thermal conductivity

The method relevant here is the laser flash method. A flat sample is heated up with a short laser pulse for ≤ 1 msec. The heat propagates though the thickness of the sample, which causes the other side to become hotter. This change in temperature is measured as a function of time, using an infrared detector. The measurement is repeated many times. Thermal diffusivity a and specific heat c_p can be determined from these measurements. Thermal conductivity can then be found through the following equation [30,8]:

$$\lambda(T) = a(T) \cdot c_p(T) \cdot \rho(T),$$

where $\rho(T)$ is the mass density of the sample.

To measure the thermal diffusivity and the specific heat of a sample in the manner described, a certain type of instrument can be used [30]. Figure 4.4 shows how a Netzsch instrument is built up. The sample is placed inside a sample carrier, and inserted into the instrument. Inside the instrument, the sample can be placed in a vacuum, or an atmosphere of choice. It has a laser that shines on the sample from below. The sample becomes hotter on the upper side, which is detected by the infrared detector above it. The sample must often be sprayed with carbon, to avoid back reflection of the laser light. The signal detected by the detector can be amplified and sent to the computer for analysis. A furnace surrounds the sample, which can allow measuring the sample's properties at various temperatures.

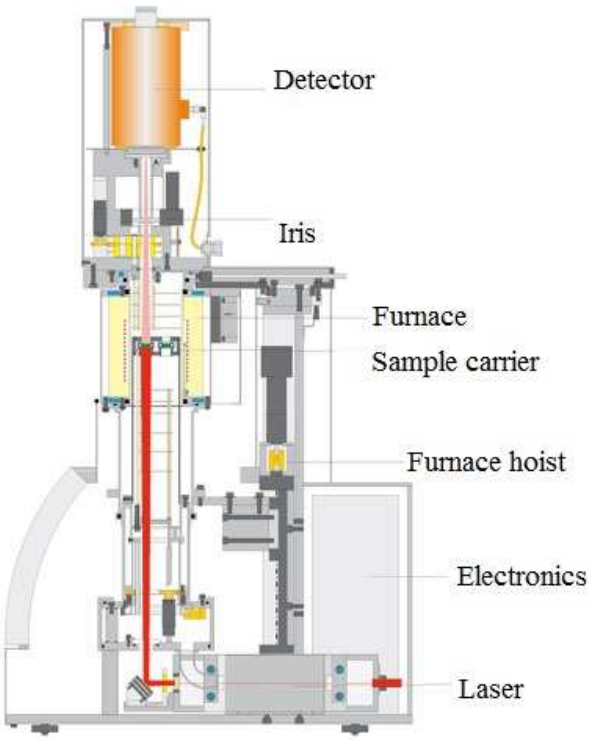

Figure 4.4: A cross-section of the Netzsch instrument for determination of thermal conductivity [30].

There are several good things about this method. First, it is not destructive. It is a non-contact method, so no material is deposited on the sample, as in the Hall measurements (the carbon can be washed away). The second advantage is that it measures thermal diffusivity absolutely, which means the method needs no calibration to determine it. However, the method still has 2-3 percent inaccuracy, which it comes from finite pulse time effects, heat losses, and the effect of non-uniform heating.

4.5.3 Seebeck coefficient

The Seebeck coefficient of a material is the thermoelectric voltage that it produces per degree temperature difference between the ends. But as mentioned in chapter 1, it is impractical to determine the Seebeck coefficient directly. To measure the thermoelectric voltage, one needs contacts, which connect a voltmeter to the sample. Figure 1.1 from chapter 1 shows how it is done. Material A is then the material whose Seebeck coefficient we wish to find, while B is the contact material with a known Seebeck coefficient α_B. Material A is subjected to a temperature gradient ΔT by two heaters. These heaters can be programmed to subject the sample to a constant temperature difference.

During one single measurement, the heaters heat the sample to a specific temperature, with a fixed ΔT between the sides (or ends) of the sample. The thermoelectric voltage is measured. Then the temperatures switch sides, although the temperature difference remains the same. Another measurement of the voltage is taken. The Seebeck coefficient of the two measurements is

$$|\alpha_{AB}| = \frac{(|V_{measured,1}| + |V_{measured,2}|)/2}{\Delta T}$$

The true Seebeck coefficient of the sample is $\alpha_A = \alpha_{AB} - \alpha_B$ (α_B is assumed to be negative in this thesis). The true α_A will be positive for a p-type material and negative for an n-type.

If the heaters can be programmed to create different temperatures, then the experiment can also give us $\alpha_A(T)$, the temperature dependence of the Seebeck coefficient.

Chapter 5

The Specific Experimental Methods

In this chapter, the actual performed experiments will be described. The specific instruments and chemicals will be mentioned.

5.1 Initial preparation of the samples

It is necessary to produce single silicon crystal samples and polycrystalline silicon with the same doping concentrations. The samples should be suitable for measurement of thermoelectric properties. The polycrystalline samples should also be suitable for microstructure characterization.

5.1.1 Preparation of single crystal silicon samples

Single crystal silicon wafers were bought from http://www.universitywafer.com/ . The following information was attached to the batch:

Name	Prime Silicon wafers
Diameter	100 mm
Resistivity	0.01 – 0.02 Ωcm
Doping	p-type, B-doped
Orientation	(100)
Thickness	510 – 540 µm
Polished	1 side is polished

Table 5.1: Information attached to the batch of wafers sent. Some information is omitted, as it isn't relevant to this master thesis (f. ex. batch number).

To prepare the single crystal samples, a wafer was cut with a diamond pen into approximately 10mm x 10 mm squares. That is the shape and size of one of the sample holders in the equipment that measures thermal conductivity. Tweezers were used to pick up the silicon bits. Afterwards, a square sample slightly larger than 10mm x10 mm was glued to a metallic rod, whose end was exactly 10mm x 10 mm. Crystalbond glue was used. The edges of the silicon

sample were ground with the #1200 grinding paper, until the sample fit neatly within the edges of the metallic rod. The glue was washed off with acetone. Then the sample was left on a piece of paper to dry. The thickness was measured with a digital micrometer.

5.1.2 Preparation of polycrystalline silicon samples

To prepare the polycrystalline samples, two single crystal wafers were crushed, milled and sintered, one wafer at a time. In the following few paragraphs, I will describe how each wafer was handled. For crushing, a mortar and a pestle of agate, and gloves were used. For ball-milling, a steel cup and 25 steel balls were used. While the original plan was to use balls and a cup of agate, they were not easily available at the time. The settings for the ball-milling machine were as follows. The time for milling was one hour. Speed was 400 rpm. The machine was set to mill for five minutes, rest for one minute, and repeat the process until one hour was over.

After the milling was over, the steel cup contained the 25 steel balls and the fine silicon powder. Because sintering of the powder was to happen the next day, it was placed inside a glove bag, along with a few other objects: some tissue paper (to protect the glove bag against sharp metal edges of the steel cup), a cold press and a spatula. The closed glove bag was connected to an argon gas source and an air pump. The setup is shown in figure 5.1:

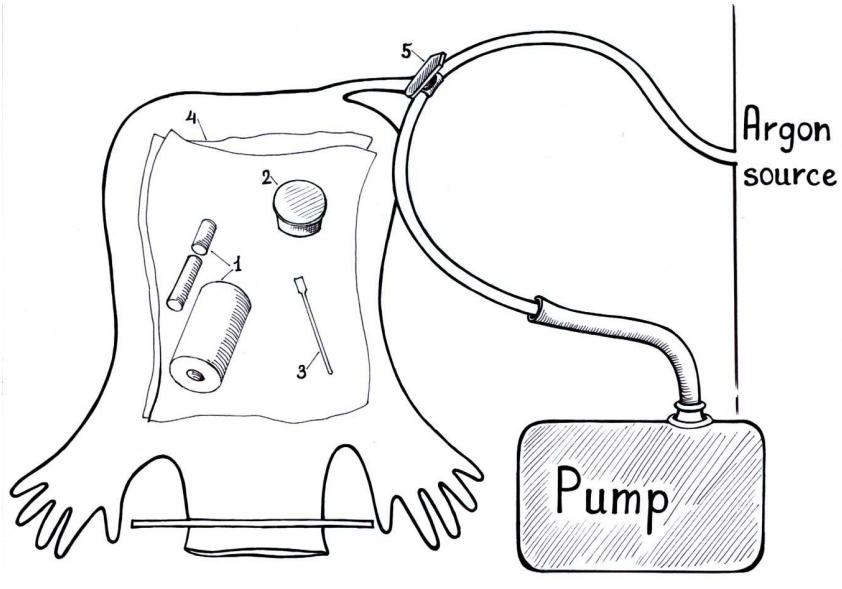

Figure 5.1: The setup for using the glove bag. The cold press (1), the steel cup with the silicon powder (2), the spatula (3) and an amount of soft paper (4) are placed inside the plastic bag. The switch (5) can be turned, to either let argon in, or pump the air out.

Argon was let into the bag, and then all gas was pumped out. This procedure was repeated once more. Then the bag was filled with argon again, and the glove bag setup was ready.

Inside the glove bag, I took the steel balls out of the steel cup, and carefully poured the remaining powder from the cup into the cold press. The cold press was taken out of the bag, and the powder inside it was pressed with the pressure of one ton for a few seconds. The result was a cylindrical, but very loose sample, threatening to fall apart at any moment. It was put inside a plastic container and then into a desiccator. The desiccator was connected to the air pump, and evacuated. The sample was kept there, until the sintering instrument was available.

Both samples were sintered using the sintering instrument Degussa, which was situated in the Chemistry building. It is unfortunately hard to control the temperature in that machine exactly. The first sample was planned to be heated room temperature to 300°C using 25 minutes, then held at 300°C for five minutes, then heated to 900°C using 40 minutes, held at 900°C for half an hour, cooled to 300°C using 40 minutes and then finally cooled to 0°C using another 20 minutes. However, when temperature was near 900°C, we observed that the sample was barely reduced in volume, which meant sintering wasn't going too well. We made a quick decision to change the top temperature to 1000°C, and hold it for 90 minutes. The final plan is summed up in figure 5.2:

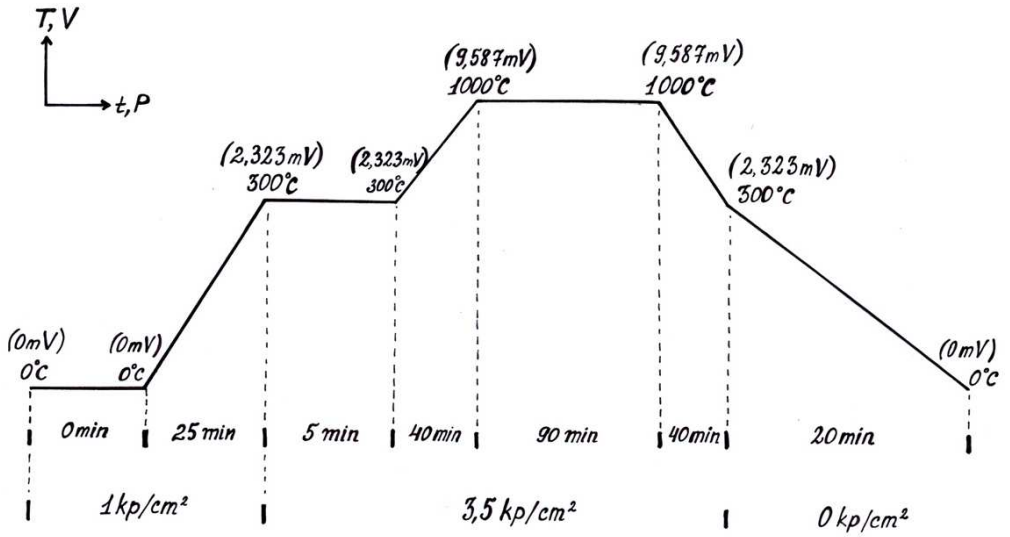

Figure 5.2: The sintering plan for the first sample.

The second sample was planned to be heated from room temperature to 300°C using 25 minutes, held at 300°C for 5 minutes, heated to 1200°C using 40 minutes, held at 1200°C at 30 minutes, cooled to 300°C using 40 minutes and then finally cooled to zero using 20 minutes. However, when temperature reached 1200°C, we saw that the sample wasn't reducing in volume well enough, and we changed the settings – top temperature was 1300°C. The final plan is summarized in figure 5.3.

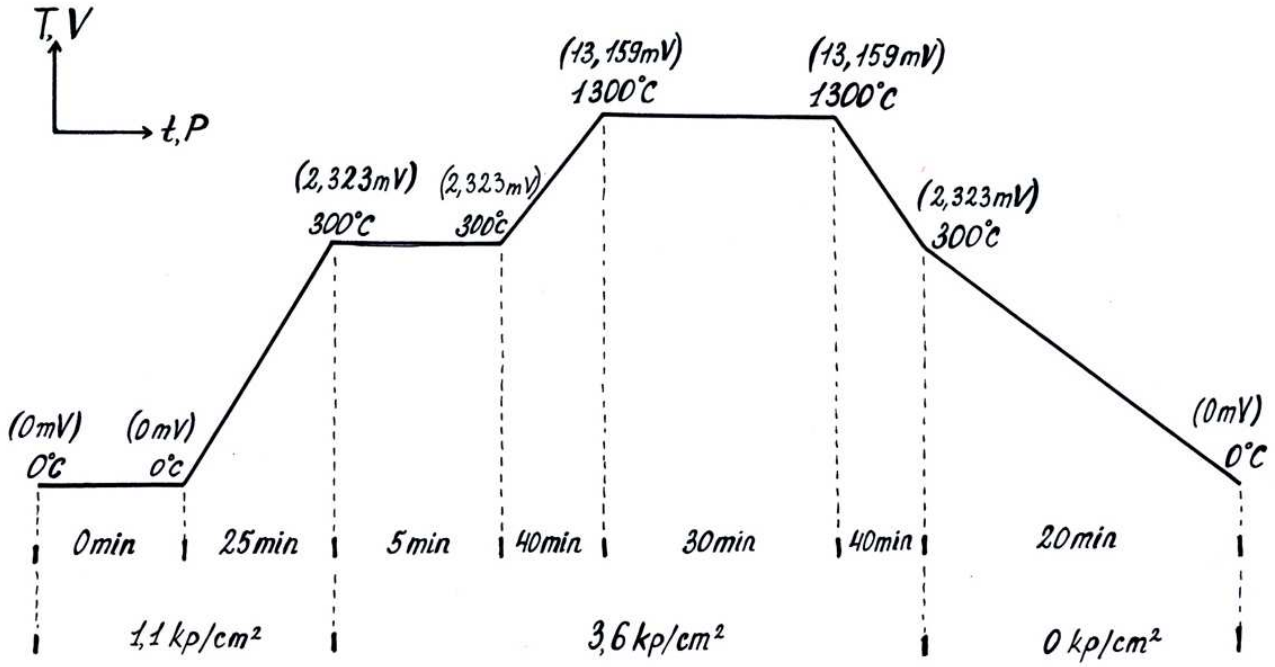

Figure 5.3: The sintering plan for the second sample.

After this procedure, this second sample was taken out of the sintering instrument. It looked like a short cylinder. Its top and bottom sides were polished with #500 grinding paper, which made them flatter and more even. After grinding, the sample was rinsed in ethanol and left on a paper to dry.

To be suitable for all the electrical measurements, the cylinder had to be cut into a flat 10mm x 10mm square. First, the cylinder had to be molded into some resin, to make cutting easier. 9 g Demotec 33 powder and 6 g Demotec 33 liquid were mixed in a plastic cup and stirred with a wooden stick. It was quickly poured into the plastic shape together with the silicon

sample. The resin soon became solid. It was taken out of the plastic shape and top and bottom were ground with 220# grinding paper, to make them flatter. Then the resin containing the sample was placed in a sample holder for the Accutom-2 cutter. It helped to pack the sample between two pieces of soft brown fabric first – it protected the sample from fracturing under the pressure from the sample holder. A Struers 356 CA saw was used. A square was first cut out of the sample. This square was around 6 mm thick, so it could potentially be cut in two, and give two 3 mm thick square samples. It was again molded into a green Demotec 33 resin, and cut with Accutom-2 as suggested. The resin was dissolved with acetone, which depending on the size of the resin bit, can take more than one day. The samples were then rinsed in acetone two more times, and at last, rinsed with isopropanol.

To create a polycrystalline sample for all the electrical measurements, a sample needed to have uniform thickness and be 10mm x 10mm in area. One of the flat square samples was glued onto a cylinder-shaped metallic piece with Crystalbond glue. The metallic piece was placed inside a ring-shaped holder. The sample was then polished with 1000# and 1200# paper manually. The sample holder described allows its user to create a uniformly thick sample. It is shown in figure 5.4:

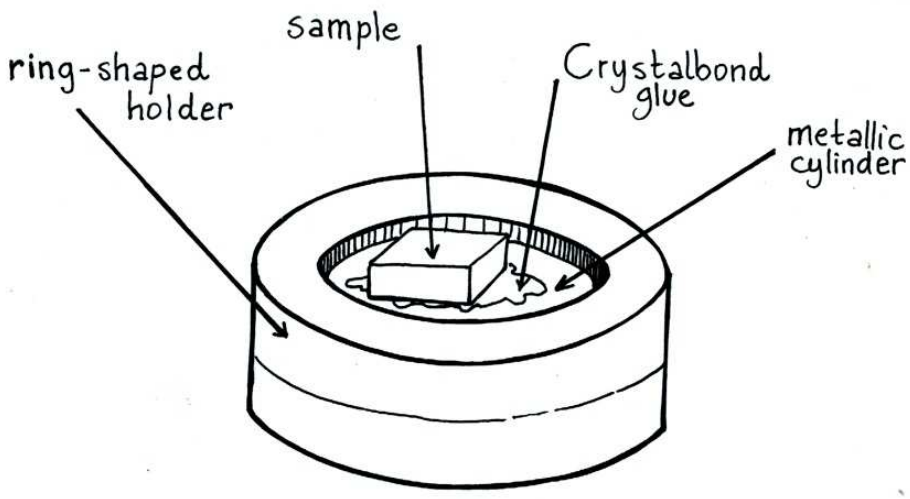

Figure 5.4: The ring-like sample holder than allows the user to grind a sample to a uniform thickness, manually.

Afterwards, the same was done to the other side of the square sample.

When the sample thickness was fairly uniform, the sample was glued onto the tip of a long metallic rod. The tip was shaped as a 10mm x 10mm square. The sample was held against the grinding paper (1000#), until its dimensions were reduced to 10mm x 10mm. Then, the sample was rinsed in acetone and left to dry. This sample was used for Seebeck and thermal conductivity measurements.

For the rest of the electrical measurements, the same sample was modified somewhat. It was ground down in thickness, until it was about 0.5mm. 1200# and 4000# papers were used, as well as the holder from figure 5.4.

5.2 Measuring the density and porosity of the samples

The sample that was sintered at 1000°C was not useful. The sample sintered at 1300°C was used for all the subsequent measurements. Porosity measurements were done on this sample both before and after it was cut into smaller pieces.

5.2.1 The geometric method

The single crystalline 10mm x 10mm sample was weighed, and its thickness was measured.

To measure the second polycrystalline sample's density, the geometric method was used. The sample was a short cylinder. The sample's dimensions and mass were measured. To measure the thickness and diameter, a digital micrometer was used. The mass of the sample was measured with the Sartorius scale designed for measuring the weight of small samples precisely. Then, the sample's volume and density were calculated with these equations:

$$V = \pi r_{av}^{2} t_{av}$$

$$\rho = \frac{m}{V}$$

Here, r_{av} is the average radius, t_{av} is the average thickness, and m is the mass.

The same method was later used on a smaller piece of this sample. It was a polycrystalline sample, with all sides at right angles. Its volume was therefore calculated with the equation $V = s_1 s_2 s_3$, where the s are the side lengths.

5.2.2 The Archimedes method

Four polycrystalline samples were used for this method. The first one, which will be called sample 1, is the short cylinder created by the sintering method alone. This sample was first weighed on a regular scale, in air. Ole Bjørn Karlsen came up with a new idea for how to measure the weight of the sample in water. The setup is shown in figure 5.5. A glass was filled with water, and held in room temperature for a while. Then the water temperature (T_w) was measured with several thermometers, as density of water varies with temperature. The density for water (ρ_w) at the specific temperature was looked up in a book (table 6-7 in CRC Handbook of Chemistry and Physics, 89th edition). Density of single crystalline silicon (ρ_{Si}) was looked up in a database [31]. A small table on three legs was constructed. It also had a small hook in the middle, from which a sample would be hung. The sample was tied to a copper thread. The table was put on the scale. Then the dry sample was hung on the hook, and the whole construction (a mass which will be called $M+_{air}$) was weighed. Later, the glass of water was brought in from the side. Unfortunately, it was difficult to hold the glass with a stand and a clamp, as depicted in figure 5.5. Instead, Ole Bjørn or I held it, while I noted the mass on the display. The first appearing mass was written down, because the sample started quickly soaking up the water and getting heavier. The mass will be signified with the symbol $M+_{water}$.

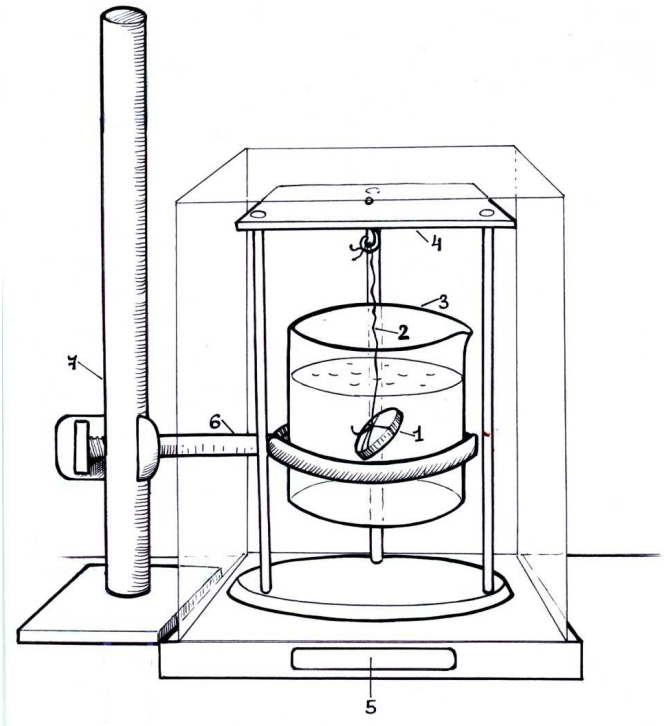

Figure 5.5: The setup for the Archimedes method. A wooden table (4) is placed on a scale. The sample (1) is attached to a copper wire (2), which is attached to the hook. A glass filled with water (3) is brought in, held by a stand (7) and a clamp (6). The weight is read off the display (5).

Because the sample was so big, a lot of wire was used, which undoubtedly made a difference and can't be neglected. The mass of the copper wire that went underwater was also measured, in air. This mass will be called $M_{Cu,w}$.

All the measurements were also repeated with three smaller samples, which were created by cutting the big sample in figure 5.5 into pieces. They will be called sample 2, sample 3 and sample 4 in chapter 6.

After all the measurements, the necessary calculations were made. To find M_{water}, the following equation was deduced from the available data:

$$M_{water} = M+_{water} - M+_{air} + M_{Cu,w} + M_{air} - (M_{Cu,w} \text{ if it was measured in water})$$

All the values in this equation are known, except for the last one. The part of the copper wire that went underwater was not measured in water, but in air. To find out what this wire would weigh in water (a value I will call $M_{Cu,w,w}$), the Archimedes principle was again used. If the wire piece is weighed underwater, the forces acting on it create this equation:

$$M_{Cu,w,w}g = m_w g + M_{Cu,w}g = V\rho_w g + M_{Cu,w}g$$

Also, the volume that the underwater wire takes up is $V = M_{Cu,w}/\rho_{Cu}$, where ρ_{Cu} is the density of copper. Using these equations, it's possible to find that

$$M_{water} = M+_{water} - M+_{air} + M_{Cu,w} + M_{air} - (M_{Cu,w} \text{ if it was measured in water})$$

$$= M+_{water} - M+_{air} + M_{Cu,w} + M_{air} - (\frac{M_{Cu,w}}{\rho_{Cu}}\rho_w + M_{Cu,\,w})$$

$$= M+_{water} - M+_{air} + M_{air} - \frac{M_{Cu,w}}{\rho_{Cu}}\rho_w$$

5.3 Characterization of microstructure of the polycrystalline samples

5.3.1 The polycrystalline samples under the optical microscope

The polycrystalline sample was observed under the optical microscope both before and after cutting it into smaller pieces. To make viewing easier, the samples were polished. Sometimes grinding paper of up to #4000 was used. Sometimes 1 µm diamond particles were also used. After that, the samples were taken to the Rechert-Jung MeF3 optical microscope, which is found in the research park. Pictures were taken using 10x, 20x, 100x and 50x lenses. Sometimes the Multifocus function was used. It's an tool that improves blurriness pictures might have due to height differences in the sample. It allows the user to take pictures at various levels, and puts them together. It was also possible to use the optical microscope to estimate the depth of holes in the surface of the samples, by using the focus screw.

5.3.2 The polycrystalline samples under the scanning electron microscope

Two SEM instruments were used. The first one was TM3000. A small piece of the polycrystalline sample was placed on some conductive putty, which was placed on a sample holder. The sample was not covered with a layer of carbon. The sample holder was placed inside the SEM. Pictures were taken at 5 and 15 kV acceleration voltage.

The TM3000 SEM was also used to observe a small piece of the unsuccessful sample, which was sintered at 1000°C. The piece was not covered with a conducting layer of carbon.

The second SEM instrument was used to look at a different sample. It was a much better polished polycrystalline sample. Low vacuum was used, because of concerns that the sample wouldn't be conductive enough. Several pictures were taken at various magnifications. EDS was used for qualitative and quantitative element analysis.

5.3.3 Transmission electron microscopy of the polycrystalline sample

TEM analysis requires a very thin sample. To prepare a thin polycrystalline silicon sample, a small flat square was sawed off, using a diamond saw and Accutom-2. Later, the square was glued to a piece of microscope glass with Crystalbond glue, and the glass was glued onto a piece of metal. The square sample was then placed under the Ultrasonic Disc Cutter drill. Some SiC powder and water was put between the drill and the sample. SiC is the material that gives the drill the ability to penetrate the sample. A breathing mask is important to use during drilling, to avoid breathing in the powder. The drill was switched on for a few seconds. After

drilling, the glass was separated from the metallic piece, and the sample was separated from the glass. The result was a circular sample, around 3 mm in diameter and 1 mm in thickness.

This circular sample was rinsed in acetone, to get rid of Crystalbond. Then it was dried on a heater, to eliminate acetone from the pores. Then one drop of Hardener G1 and ten drops Resin G1 were mixed in a Teflon cup. The sample was placed in the mixture, and the cup was placed on a heater. After a minute, the mixture hardened and changed color from transparent yellow to dark red. The excess glue was polished away manually, leaving only the small circular sample, which hopefully soaked up the glue while it was still a liquid.

One side of the sample was glued to a long glass cylinder using Crystalbond glue. The exposed side was polished with #1200 and #4000 polishing paper, plus 1 μm diamond particles. The sample was detached from the glass cylinder. A copper ring with a big hole was glued onto the polished side, using the same G1 glue. This glue needs heat to fulfill its function as glue. It also needs to spread relatively uniformly between the copper ring and the sample, so application of pressure is necessary. Therefore, a specific setup was used, shown in figure 5.6. As shown, pieces of paper surround the sample at both sides, and a metallic clamp is pressing the sample at both sides. The clamp is placed on the heater, where it is warmed up to ca. 100°C (around the 2 mark on the heater scale) and held there for ten minutes.

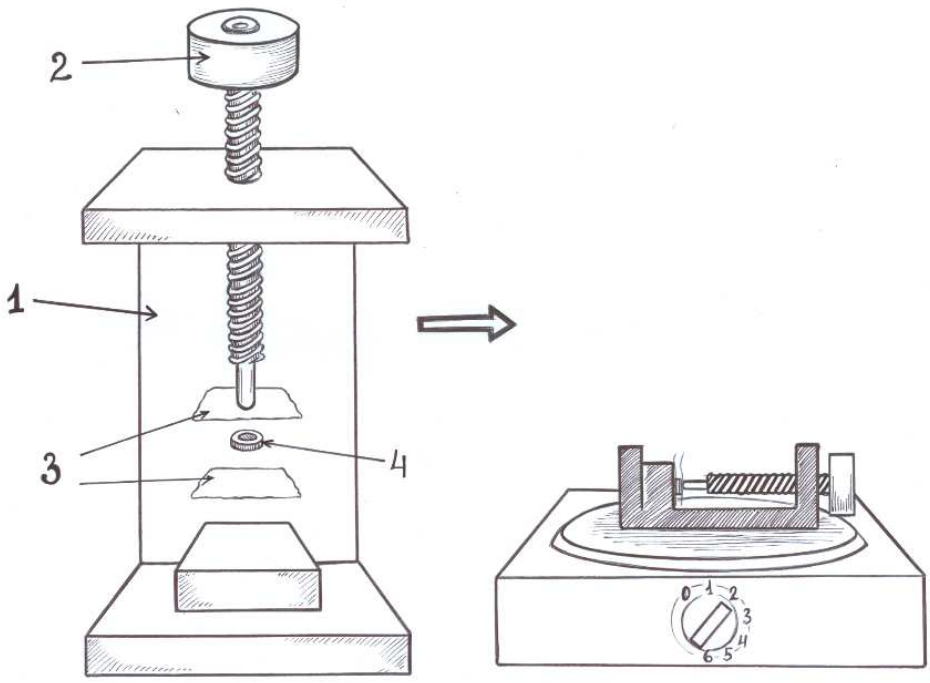

Figure 5.6: The setup for gluing the copper ring to the sample. The figure to the left illustrates the clamp (1). The sample (4) is surrounded by two pieces of paper (3), and pressed together with the screw (2) of the clamp. The figure to the right illustrates the same clamp, placed on a heater.

After this, the glue was solid. It held the copper ring and the sample together. Paper residue was manually polished away.

The sample was still ca. 1 mm thick. To thin it down to around 20 µm, the Multiprep polishing instrument was used. It allows the user to see how much of the thickness has been polished away. The plan is to reduce the thickness to 150 µm using the 30 µm particle paper, then reduce it to 60 µm using 9 µm particle paper, then reduce it to 33 µm using 3 µm particle paper. At last, the thickness must be reduced to 20 µm with 0.5 µm paper. The copper ring side of the sample was glued onto a special sample holder with Crystalbond. To know how thick the sample is, its edge was lightly polished and flattened. It is visible under the optical microscope and is shown in figure 5.7. The ProgRes CapturePro 2.7 program also allows one to measure how thick an object on the screen is.

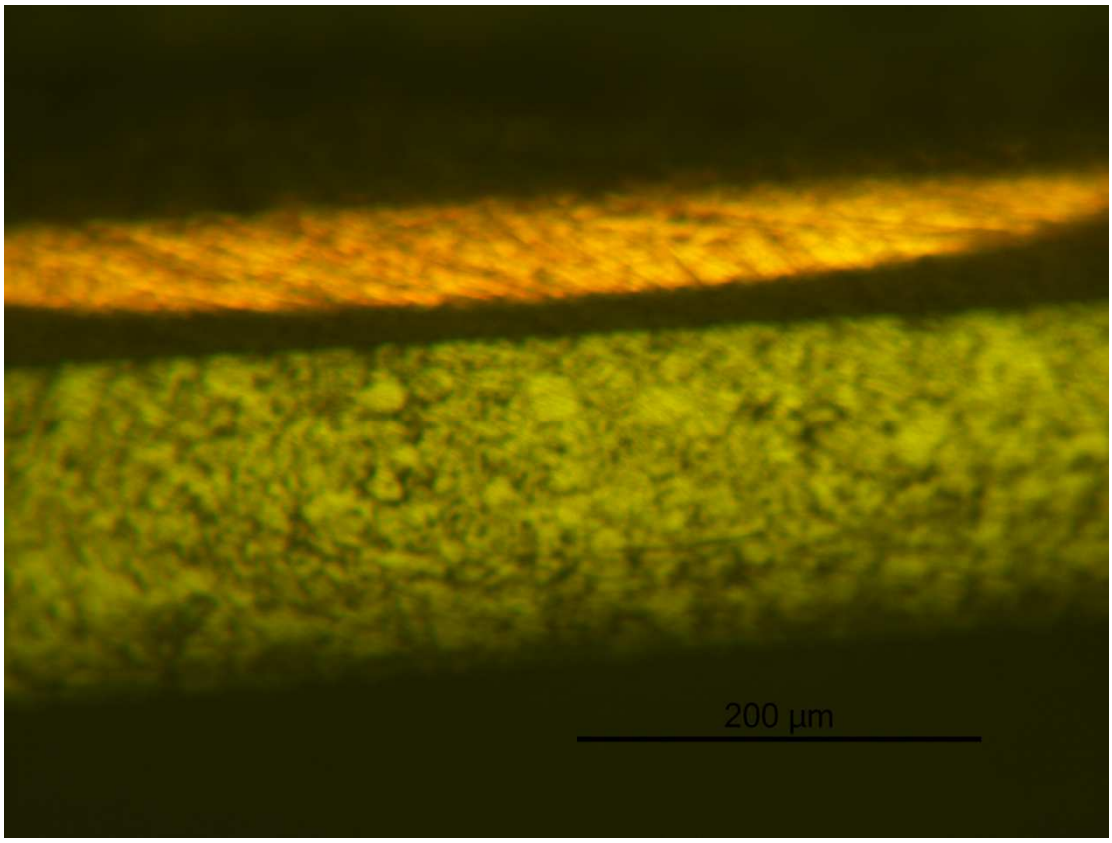

Figure 5.7: The polished edge of the TEM sample. The upper yellow strip is the copper ring. The green lowed strip is the sample edge. The sample is around 150µm thick in this picture.

The thickness was reduced to 150µm with 30µm-partide paper, as planned. Then 9µm-particle paper was used. Unfortunately it was very old, and polishing away only 5µm per 30 minutes, so a brand new one replaced it. Unfortunately, it was too new, and ground down the sample to 40µm thickness in a matter of seconds. Then the sample was polished with 0.5µm paper for a few seconds. Then the sample was detached from the Multiprep sample holder, and held in acetone for a few minutes.

Then it was prepared for ion polishing. The PIPS (Precision Ion Polishing System) instrument was used. It shoots the sample with argon ions. The sample was mounted in the sample holder with its copper ring up. The ion beams were set to bombard the sample from both sides, at the incident angle of 6°.The rotation speed was chosen to be 5rpm, and the acceleration voltage for the ions was 5 keV. The option "Double" was chosen, so that both ion beams are off, when they pass the two clamps that hold the sample in place. This is to avoid grinding down the clamps. The camera was held above the sample while it was milled, which helps monitor the hole-formation. It took five hours and five minutes to form a small hole.

The sample was then ready to be inserted into TEM. The TEM used in this work was the Jeol JEM-2000EX. This microscope doesn't allow the user to obtain digital images of the sample directly. One has to take several photos, develop them, and then scan them with a regular scanner.

First, some liquid nitrogen was poured into cold trap. This cools the rods around the sample, which allows them to trap moisture evaporating from the sample, and preserve a good vacuum inside the microscope column. It is important to cover the microscope screen with a lid, while pouring the nitrogen. Then the sample was placed inside the sample holder pole, and held in place with a small ring-like screw. The sample holder pole was inserted into the microscope column according to the manual. Then some more nitrogen was poured into the cold trap. When the pressure inside the column reached the 10^{-5} Pa scale on the pressure-meter, the CRT Intensity screw was used to turn on one of the displays. The display showed that the acceleration voltage for electrons was set at 100kV. The red "HT" button was pushed to turn on the acceleration voltage, which went straight to 100kV. Then the voltage was increased to 180kV with the rate of 1kV per 5 seconds. It was then raised to 200kV with the rate of 1kV per 15 seconds. The screw that increases the filament temperature was slowly turned from zero to four with the rate of one step per minute, and then to six with the rate of half a step per

minute. The beam was found at low magnification, by varying the brightness and using diffraction mode.

Then, certain alignments were made:

1. Gun tilt and shift correction. This procedure puts the electron beam along the z-axis of the column.
2. Condenser lens: centering of the condenser aperture and correction of the astigmatism of the lens.
3. The sample was brought into the eucentric height of the objective lens.

Attempts were made to correct the objective lens astigmatism, but it did not work. All this work took many hours, so the liquid nitrogen was again refilled. After that the microscope was finally ready for observations of the sample. 15 bright field images were taken. To shut down the TEM, the filament temperature screw was turned to zero, and the acceleration voltage was decreased back to 100kV. This time, it was not necessary to do it slowly. The red "HT" button was pushed to shut off the acceleration voltage completely. The lid was put back onto the screen.

The drawer containing the picture slides was opened. It contained two boxes: one with the remaining 35 unused photo papers, and one with those containing the pictures of the sample. The two boxes were taken out, and were replaced by two other boxes: one with 50 unused photo papers, and another completely empty. The original two boxes were taken to the photo-developing room. The box with 35 unused papers was refilled with 15 extra unused papers. The 15 pictures of the sample were put in first developer liquid for five minutes, rinsed, held in second developer liquid for 10 minutes, and then held in rinsing liquid for half an hour. Then they were taken out and left to dry on a piece of paper.

5.4 Electrical characterization of the samples

Electrical characterization was done on both single crystal silicon and on the polycrystalline sample.

5.4.1 Measurements of thermal conductivity

Thermal conductivity of the single crystalline sample was measured first. The 10mm x 10mm x 550 µm square sample was taken to MiNa-Lab, where the Netzsch LFA 457 *MicroFlash*

instrument is found. It measures thermal diffusivity with ±2-4 % margin of error. The manual for its use was followed, and is always found on the table nearby. The sample was sprayed with carbon, and put into the third sample seat. Reference sample (Pyroceram) was placed in the first sample seat. The second sample seat was covered with a dummy sample. Program Netzsch LFA457 was used. The first measurement was to be done at 30°C. The next measurement temperatures were programmed to be 50°C, 100°C, 150°C, and the following temperatures with the interval of 50°C, until 650°C is reached. Until 100°C, the temperature was programmed to increase by 2 K/min. Between 100°C and 650°C, the temperature was programmed to increase by 3 K/min. Once everything was set up, the measurements were commenced, and they took a day. Next day, they were finished, and the sample was taken out. It was still covered in carbon, so it was cleaned in acetone, inside an ultrasonic cleaner. The data collected overnight were used in the program-assisted calculation of specific heat capacity, and thermal conductivity. Unfortunately the reference sample and the experimental sample were covered with different lids. The lids had different holes on them. The program warned of the possibility that calculation of specific heat would be less accurate.

The polycrystalline sample later went though the same procedure. Its dimensions were 10.5mm x 10.75mm x 2.765mm.

5.4.2 Measurements of effective resistivity, charge carrier concentration and Hall mobility.

To measure these properties, a Temperature Dependent Hall (TDH) instrument was used. It is found in the cleanroom in the MiNa-Lab. It is named LakeShore 7604, and can find all the properties listed in the title while varying temperature from 10 K to 350 K [32]. Magnetic fields it can produce are 1.0 to 1.3 T. It's suitable for measuring carrier concentrations between 10^6 to 10^{19} cm^{-3}, and mobilities between 1 and 10^5 cm^2/Vs. It uses the van der Pauw four-point probe method.

The single crystalline sample was tested first. The procedure was done according to the manual. The first sample was a square piece of the silicon wafer, not used in any other tests. It was smaller than 10mm x 10mm, and its thickness was 540µm. The sample was placed on the sample holder rod with some double-sided tape. The four thin wires of the rod were soldered onto the corners of the sample with Indium. After soldering, each wire was gently pulled with tweezers, to check if they were firmly attached to the sample. Then resistance between each

pair was measured. If resistance between a certain pair was higher than all the others, that pair was resoldered to the sample, until the resistances everywhere were approximately the same. Then the sample holder rod was lowered into the sample chamber. The LakeShore instrument was then used to test the resistances once more, just to make sure. For actual resistivity, mobility and carrier concentration measurements, the right current needed to be used. There are certain limits: the voltage must not exceed 3V, current must not exceed 20 mA, and the effect must not be larger than 1 mW. A current of 10 mA was chosen. Then the sample chamber was cooled to 10 K. The LakeShore program was used to program the system to do this list of tasks:

1. Warm up the sample to 70 K with the heater.
2. Create an *V* vs. *I* curve at 70 K. This step does the same as the resistance checks done two times earlier. It also shows if the behavior is ohmic or not.
3. Perform the measurements of mobility, carrier density and resistivity, as functions of temperature. It should happen between temperatures 70 K and 340 K. The temperature step between measurements was chosen to be 10K. The magnetic field was 10 kG and -10 kG.
4. Shut down the heater.

After these steps, the sample chamber was warmed to ca. 300 K again, data were saved and collected, and the sample was taken out and detached from the thin wires.

The same procedure was done with a polycrystalline sample, except different steps were programmed. The sample was 10.5cm x 10.75cm, and its thickness was 520μm. The following steps were done:

1. Go to temperature 10 K.
2. Create a *V* vs. *I* curve at that temperature.
3. Perform measurements of mobility, carrier density and resistivity as functions of temperature, until 70 K
4. Reach 70 K.
5. Create a *V* vs. *I* curve again.
6. Perform all the measurements again, as in step 3, until 330 K is reached.

5.4.3 Measurements of the Seebeck coefficients

The polycrystalline sample was the first one to undergo this experiment. It was taken to the Seebeck instrument in the MiNaLab. The sample was placed between two thin carbon plates, which were in turn placed between two copper pieces. The copper pieces were placed between glass plates, which were in turn placed between two heating elements. The setup is shown in figure 5.8.

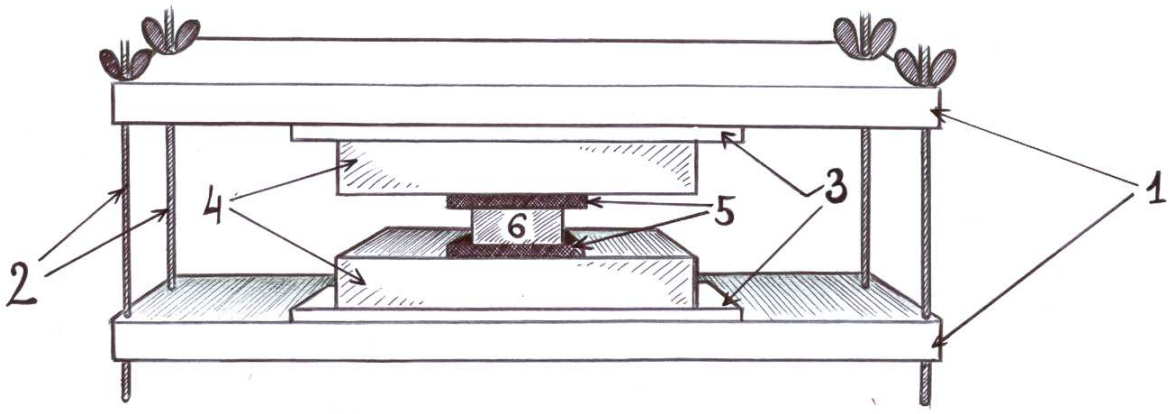

Figure 5.8: The Seebeck setup. The sample (6) is placed between carbon plates (5), copper pieces (4), glass plates (3) and heating elements (1). Screws (2) screw the heating elements together, and hold the sample firmly pressed between them. The whole setup is to be placed inside the chamber.

These layers were pressed together and fixed with screws. Then they were placed inside a chamber. It is important to place them in such a way that they don't touch the inner walls of the chamber too much. The chamber was covered with a glass dome. Air was pumped out for a few minutes. Then the nitrogen was let in, and the pump was turned off. After a minute, nitrogen flow was set to 0.5 L/min. The heating elements were plugged in: one into a regular socket, another into the UPS. One can check that both heating elements are on, by checking that both green lights are blinking. Then the Julabo water cooler was switched on, and the light blue valve was opened. This allows the cooling water to be cooled with yet another source of water. It helps avoid overheating, if the barrel of water is not enough. Then the Seebeck-Resist program was opened. Data were put in. It is summarized in table 5.2. The measurements of the Seebeck coefficient are to start at 50°C, and to end at 350°C. Temperature will increase in steps of 50 K, which means measurements will be made around

50°C, then 100°C, 150°C, etc. The sample should stay at each temperature for 120 minutes, and the temperature difference between the sides of the sample will be 6 K.

Starting temperature	50°C
Maximum temperature	350°C
Step duration (how long to stay at a specific temperature)	120 min.
Temperaure step	50K
Temperature difference	6K

Table 5.2: Important data entered into the program for measurement of the Seebeck coefficient of the polycrystalline material.

Then the “Run” button was pressed, and the measurements took a day. After they were done, two more measurements were attempted. The first was the same as the previous, only starting temperature was 350°C and the maximum temperature was 400°C. The second was also the same, except starting and maximum temperatures were both 50°C, temperature step was zero, and the carbon plates were taken out.

The single crystalline silicon sample was also tested with the same instrument. The setup is identical to the one in figure 5.8, except the carbon plates were not used. The sample was so thin that there were concerns about the accuracy of the data, in case of carbon use. It was only 550 µm thick. The thinness of the sample also made the copper pieces touch each other, which is an undesirable effect. Therefore, three nearly identical single crystal silicon samples were placed between them, for stability. It is ok to use many, as the geometry of the sample is not important [ref20]. Table 5.3 shows the data entered into the program.

Starting temperature	50°C
Maximum temperature	300°C
Step duration (how long to stay at a specific temperature)	120 min.

Temperaure step	50K
Temperature difference	6K

Table 5.3: Important data entered into the program for measurement of the Seebeck coefficient of the single crystalline material.

Chapter 6

Results

This chapter will describe the results of all the experiments from chapter 5.

6.1 Results of the synthesis

The single crystalline sample had the area 10mm x 10mm. Its thickness was not uniform. Measured in three places, it was 0.548 mm, 0.550 mm and 0.552 mm, making 0.550 mm the average thickness.

The first sample prepared by sintering a fine powder of silicon was not solid. It fell apart as soon as it was taken out of the sintering instrument. There was a lot of powder, and some bits were solid, but they were not good enough to cut and prepare for electric measurements.

The second sintered sample was solid, and did not fall apart. It has some metallic shine, unlike the previous sintered sample. The various samples made out of it were successfully prepared as well – none broke.

6.2 Density and porosity of the polycrystalline sample

6.2.1 Results of the geometric method

The successful polycrystalline sample was uneven, as shown in the tables 6.1 (thickness measurements) and 6.2 (diameter measurements). The standard deviations are written with the symbol s.

Largest thickness found	6.448 mm
Smallest thickness found	5.846 mm
The average value	6.147 mm (s = 0.4257)

Table 6.1: Results of the measurement of the cylindrical sample's thickness, and their average value. The thickest and the thinnest parts of the sample were found, and the average calculated.

Diameters	25.811 mm
	25.836 mm

	25.858 mm
	25.894 mm
	25.760 mm
	25.821 mm
The average value	25.830 mm (s = 0.045295)

Table 6.2: Results of the measurements of the cylindrical sample's diameter, and their average value.

Measurements of the mass were done right after the sample was polished with grinding paper, which soaks the sample and the grinding paper in water. It was also rinsed in ethanol. When the sample was put on the scale, it showed around 6.5 g. However, the mass on the scale was decreasing about 0.0001g per second. It could likely be due to the fact that the sample soaked up liquid, and it was evaporating. The sample was weighed the next day. The mass of the dry sample was 6.3435 g, and stable.

The volume was calculated to be 3.2211 cm^3 and density 1.969 g/cm^3. Porosity was found to be 15,46%.

Later, this sample was cut into bits, and the smaller sample was measured. Its sides were 10.75 mm, 10.50 mm and 2.765 mm. Its mass was 0.5629 g. Its density was therefore 1.804 g/cm^3, and porosity 22.56%.

6.2.2 Results of the Archimedes method

Several measurements were made during this method, and will first be summed up in table 6.3, before the results of porosity calculation is shown. Some properties in the table were looked up in tables, rather than measured (density of water, density of copper and single crystalline silicon [31]).

Property	Symbol	Value (sample 1)	Value (sample 2)	Value (sample 3)	Value (sample 4)
Weight of sample in air	M_{air}	6.3402 g	0.5618 g	0.9242 g	1.1994 g

Temperature of water	T_w	23.4°C	21.5°C	21.5°C	21.5°C
Mass density of water	ρ_w	0.9974456 g/cm^3	0.9978852 g/cm^3	0.9978852 g/cm^3	0.9978852 g/cm^3
Mass of (table + copper wire + sample), in air	$M+_{air}$	62.5534 g	55.573 g	55.934 g	56.216 g
Apparent mass (table + copper wire halfway in water + sample in water)	$M+_{water}$	59.75 g	55.31 g	55.47 g	55.64 g
Mass density of copper at room T	ρ_{Cu}	8.94 g/cm^3	8.94 g/cm^3	8.94 g/cm^3	8.94 g/cm^3
Mass of copper wire that went underwater (in air)	$M_{cu,w}$	0.0264 g	0.0106 g	0.0145 g	0.0164 g
Density of pure single crystal silicon at 25°C	ρ_{Si}	2.329002 g/cm^3	2.329002 g/cm^3	2.329002 g/cm^3	2.329002 g/cm^3

Table 6.3: Results of the Archimedes method measurements.

The temperature of the water for sample 1 was measured with four thermometers, which yielded temperatures 23.2°C, 26.5°C, 23.6°C and 22.5°C. The two of the thermometers seemed to show temperatures that were either too low or too high, so I decided not to trust them. I picked 23.4°C as the temperature of water, which is (23.2°C + 23.6°C)/2. When $M+_{water}$ was measured for sample 1, the last two decimals were fluctuating too much to be

determined correctly. The number quickly rose to by ca. 0.02g, which was probably due to sample soaking up water.

Using the equations constructed in chapter 5, porosity was found to be 3.24% for sample 1, 8.89% for sample 2, 15.0% for sample 3 and 11.1% for sample 4.

6.3 Microstructure of the polycrystalline sample

6.3.1 Results of optical microscopy

Pictures were taken of various samples at different stages of polishing. All the pictures are of the polycrystalline sample sintered at 1300°C. Figures 6.1 and 6.2 show a sample surface, which was polished with #1200 and #4000 grinding paper. The upper parts of these figures show a less polished sample, while the lower parts show a more polished one. The pictures show some scratches, which come from the polishing process. They also show what appear to be holes in the surface.

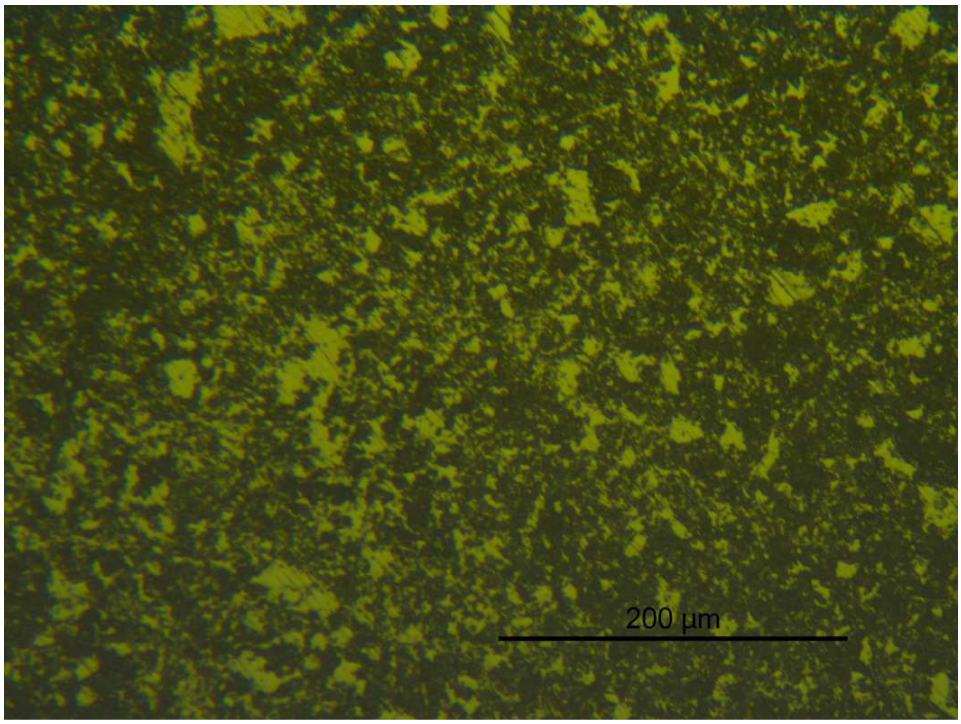

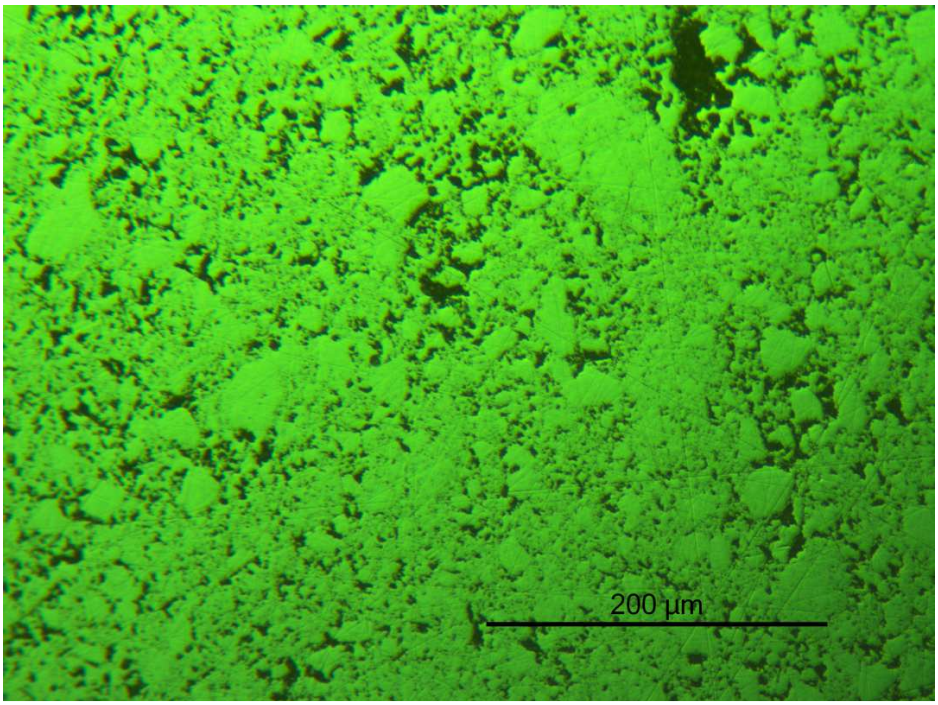

Figure 6.1: Sample surfaces of the polycrystalline sample, at different stages of polishing. Scale: 200 µm.

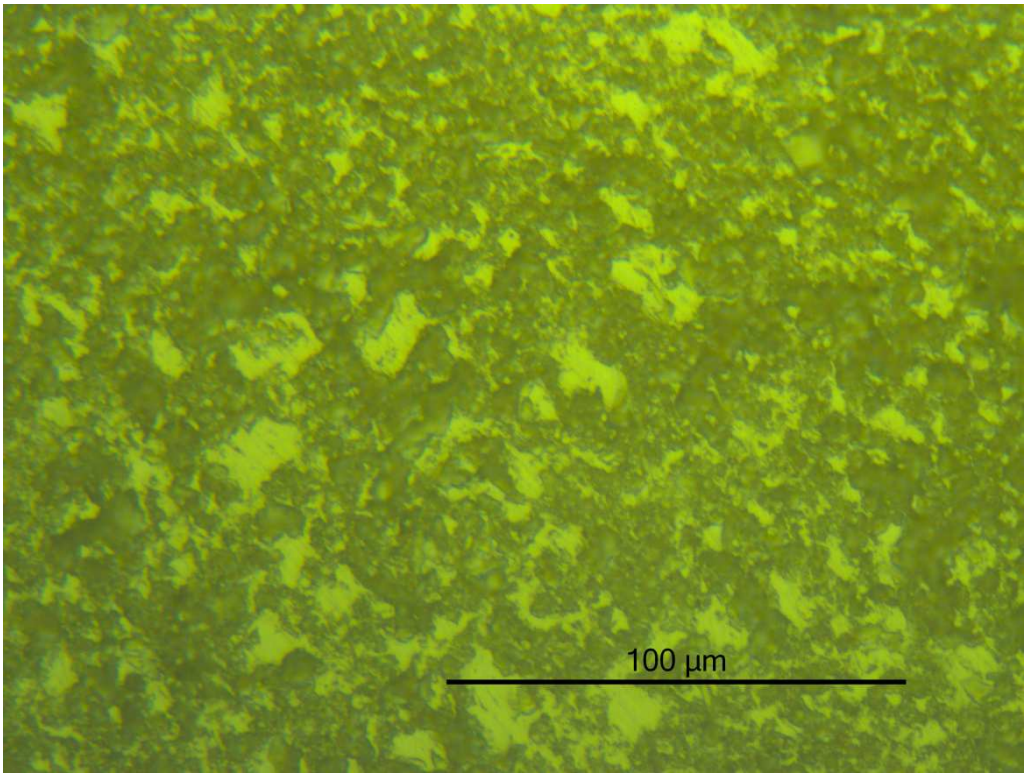

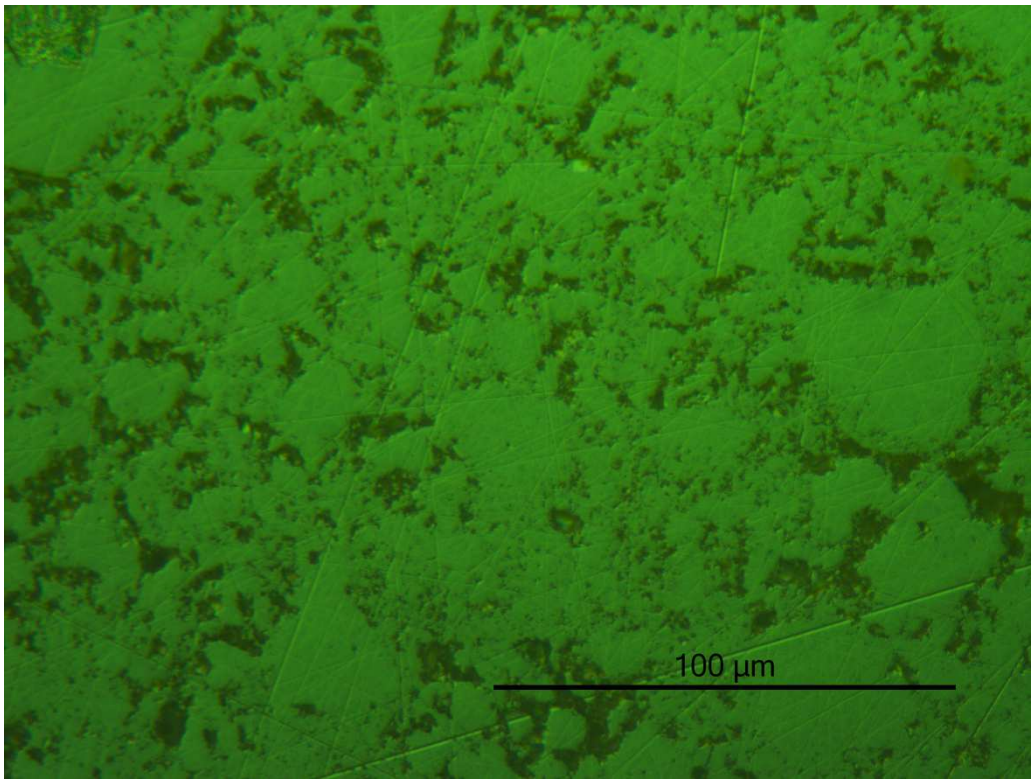

Figure 6.2: Surfaces of the polycrystalline sample, at different stages of polishing. Scale: 100 µm.

The hole size is on average 1-2 µm in diameter, when deduced from the pictures alone.

6.3.2 Results of scanning electron microscopy

The first SEM used was the TM3000. It was used to look at the successful sample. The image did appear, but it was somewhat blurry. The same instrument was used to look at the unsuccessful sample, but that produced no image at all.

The sample polished with #1200 and #4000 grinding paper was used for the second SEM. It produced good images. Figure 6.3 shows the polished surface of the sample.

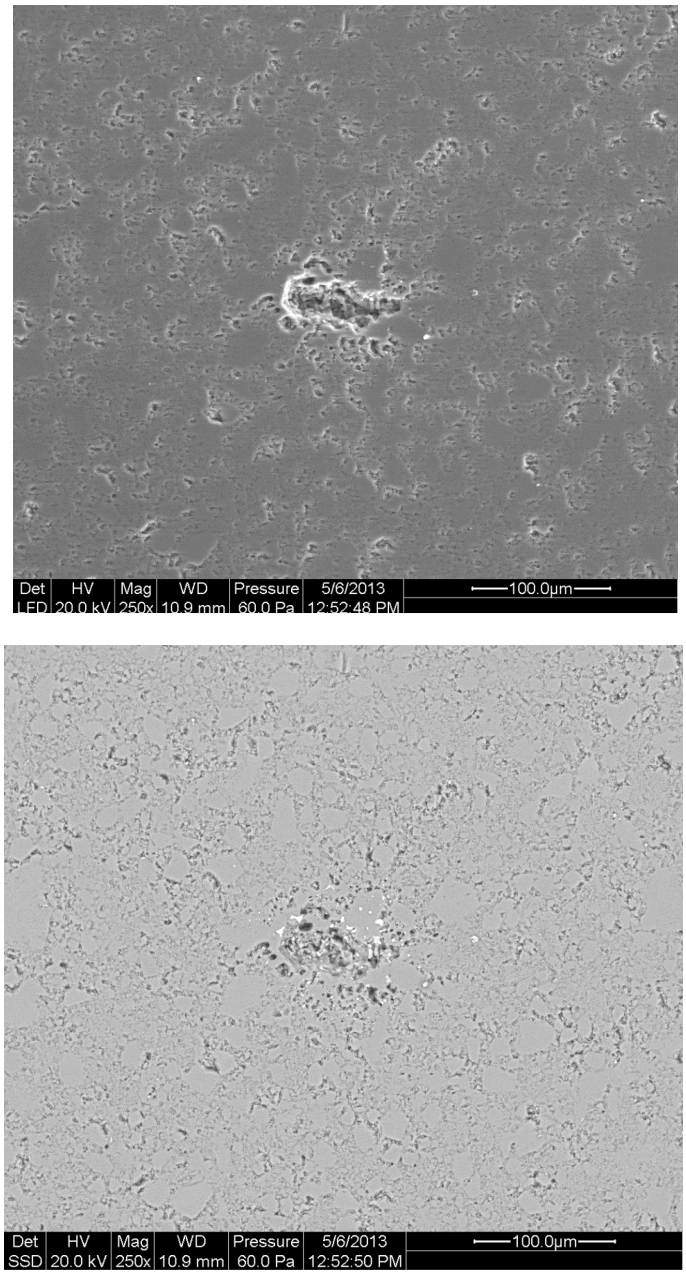

Figure 6.3: SEM images of the polished surface of the polycrystalline sample. Upper: secondary electrons (SE) image; lower: back-scattered electrons (BSE) image.

The upper image was created by using the secondary electrons (SE), which mainly create contrast due to topography. The lower image was created using the back-scattered electrons (BSE), which create a lot of its contrast due to difference in atom number.

As in the optical images, holes in the surface seem to be present. Figure 6.4 takes a closer look at the holes.

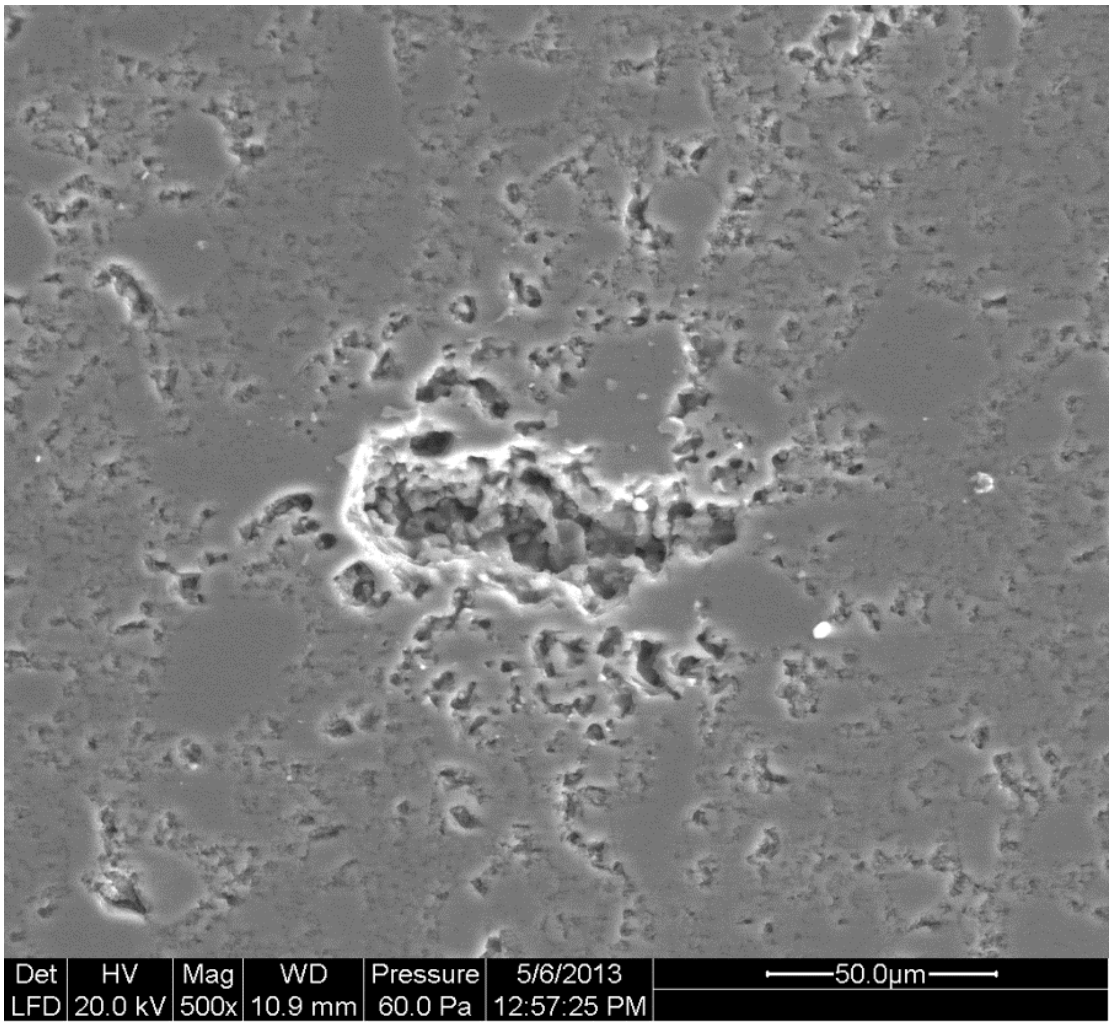

Figure 6.4: A SEM image of the surface of the polycrystalline sample, created using SE.

The holes are on average around 3µm in diameter, judging from the SEM images.

The SEM was also used to analyze which elements the polycrystalline sample contained. EDS was used on many spots on the sample. Most of the time, only the silicon peak showed up. Sometimes, iron showed up as well, as shown in figure 6.5. The figure shows several peaks, but the program only recognizes two of them. The unrecognized peaks are small. Quantitative analysis of that spot suggested that it contains 91.05 at% silicon, and 8.95 at% iron.

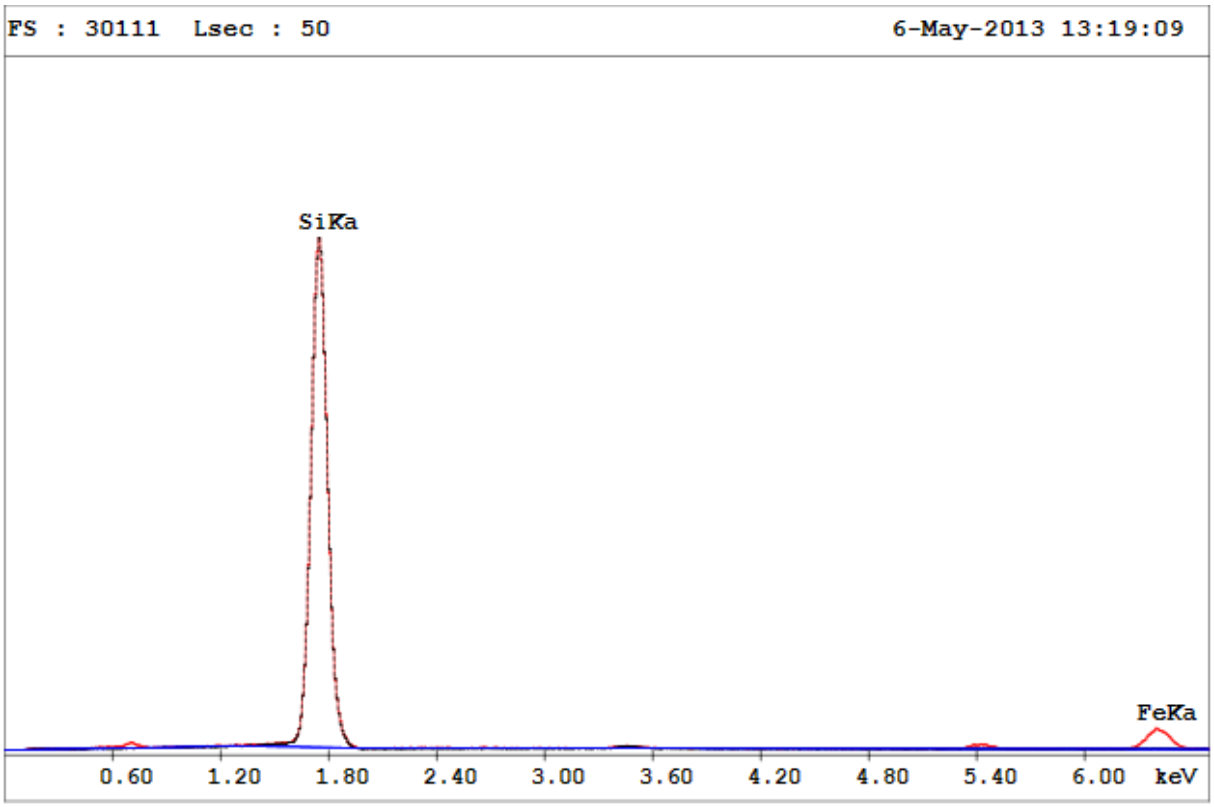

Figure 6.5: Qualitative analysis of element content in the sample, using EDS.

6.3.3 Results of transmission electron microscopy

The images were taken of the edge of the hole in the sample (figure 6.6 and 6.7).

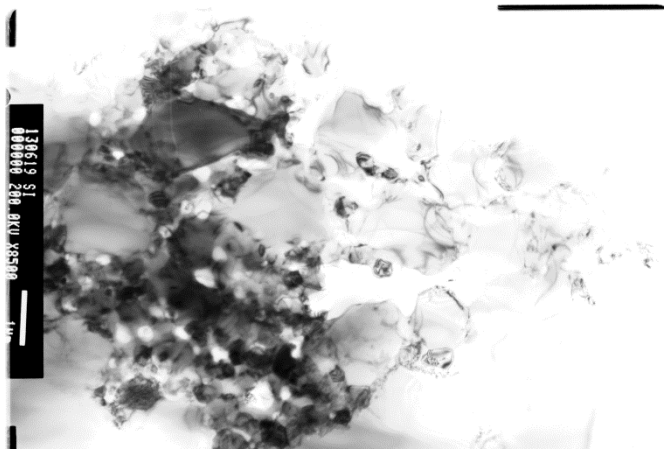

Figure 6.6: A bright field image, showing an area where small holes are visible to the left, and larger holes to the right.

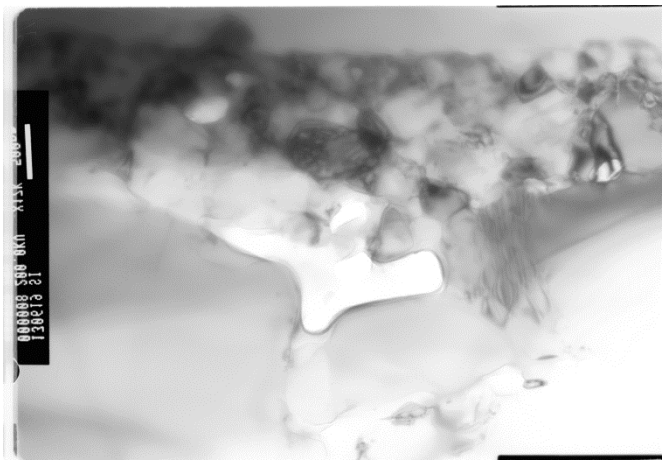

Figure 6.7: A brightfield image, showing an area where bigger holes (middle) and bigger grains to the left) are visible.

Unfortunately, many images lack a visible scale bar, and turned out too bright.

6.4 Results of electrical characterization

6.4.1 Thermal conductivity

Figure 6.8 displays results of thermal conductivity measurements of both the polycrystalline and the single crystalline samples. Figure 6.9 displays results of measurements of thermal diffusivities. Figure 6.10 shows the specific heat capacities, estimated by the Netzsch LFA 457 *MicroFlash* instrument.

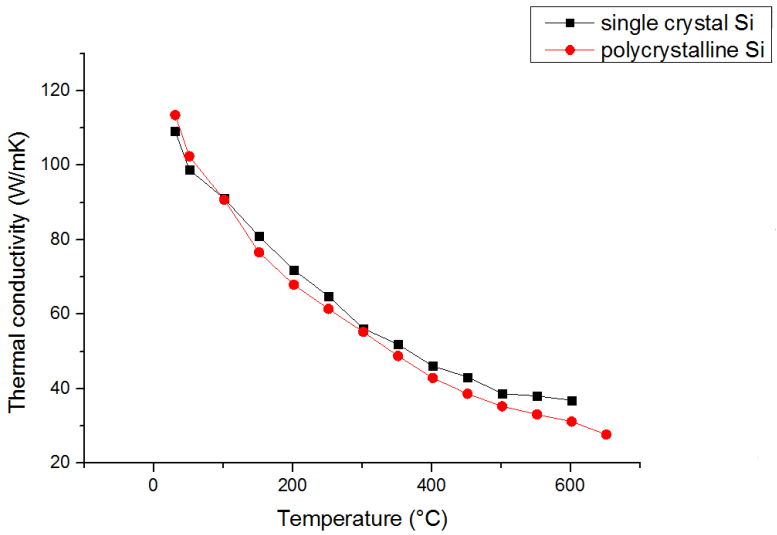

Figure 6.8: Measured thermal conductivities of the polycrystalline and the single crystalline B-doped silicon.

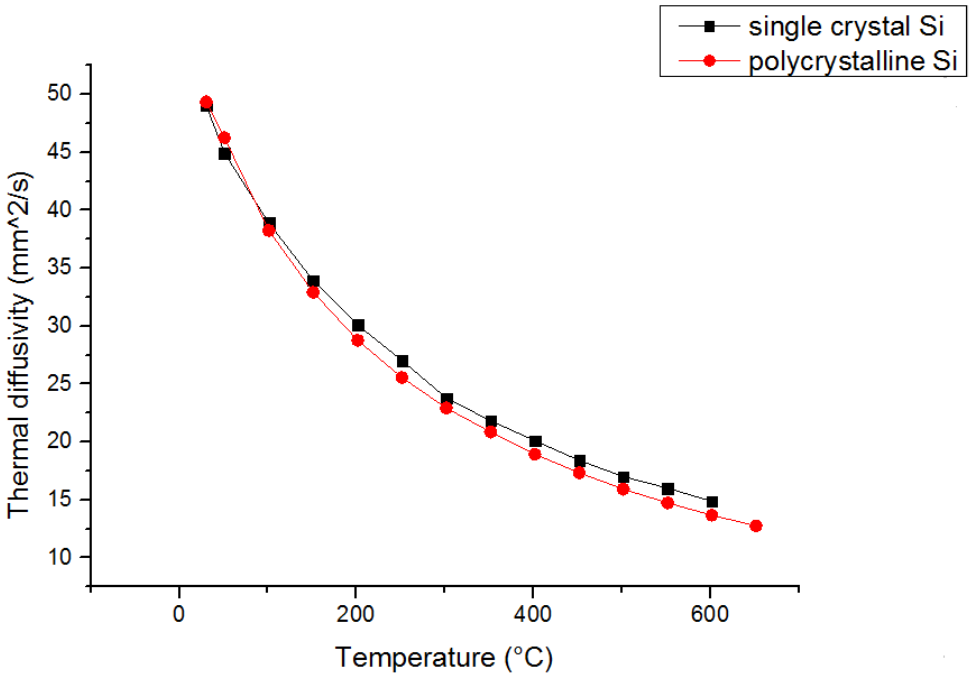

Figure 6.9: Measured thermal diffusivities of the polycrystalline and the single crystalline B-doped Si.

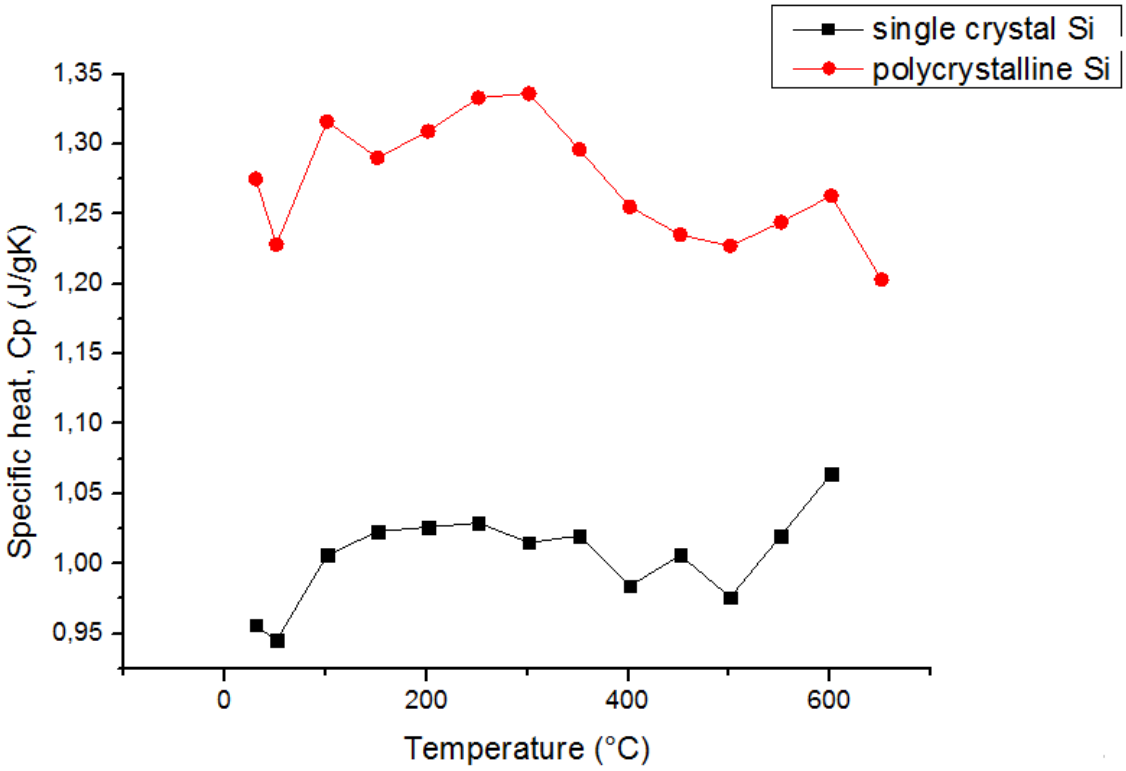

Figure 6.10: Estimated specific heats of the polycrystalline and the single crystalline B-doped silicon.

6.4.2 Effective resistivity, charge carrier concentration and Hall mobility.

Figure 6.11 shows the resistivities of the polycrystalline and the single crystalline samples. Figure 6.12 shows the Hall mobilities, and figure 6.13 shows the charge carrier concentrations. Both samples were classified as “p-type” conductors by the program.

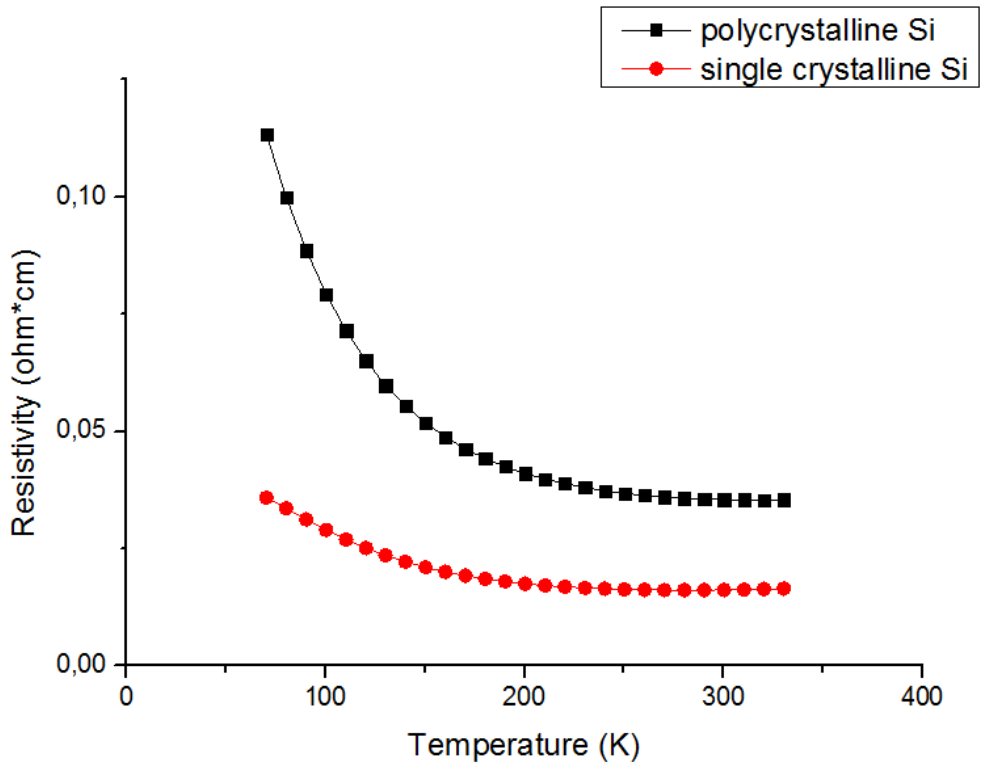

Figure 6.11: The resistivities of the polycrystalline and the single crystalline silicon samples

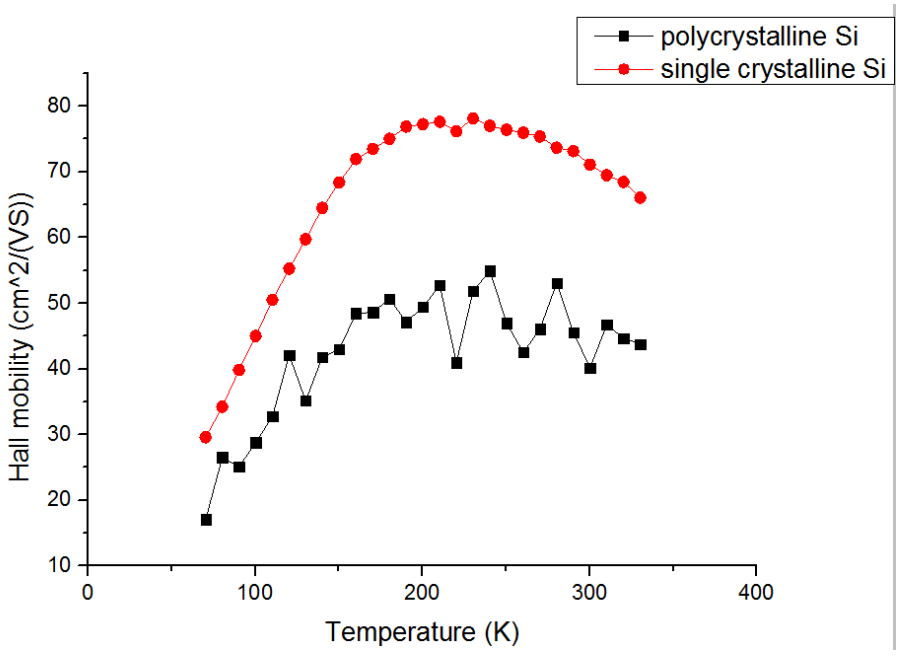

Figure 6.12: The Hall mobilities of the single crystalline and the polycrystalline silicon samples.

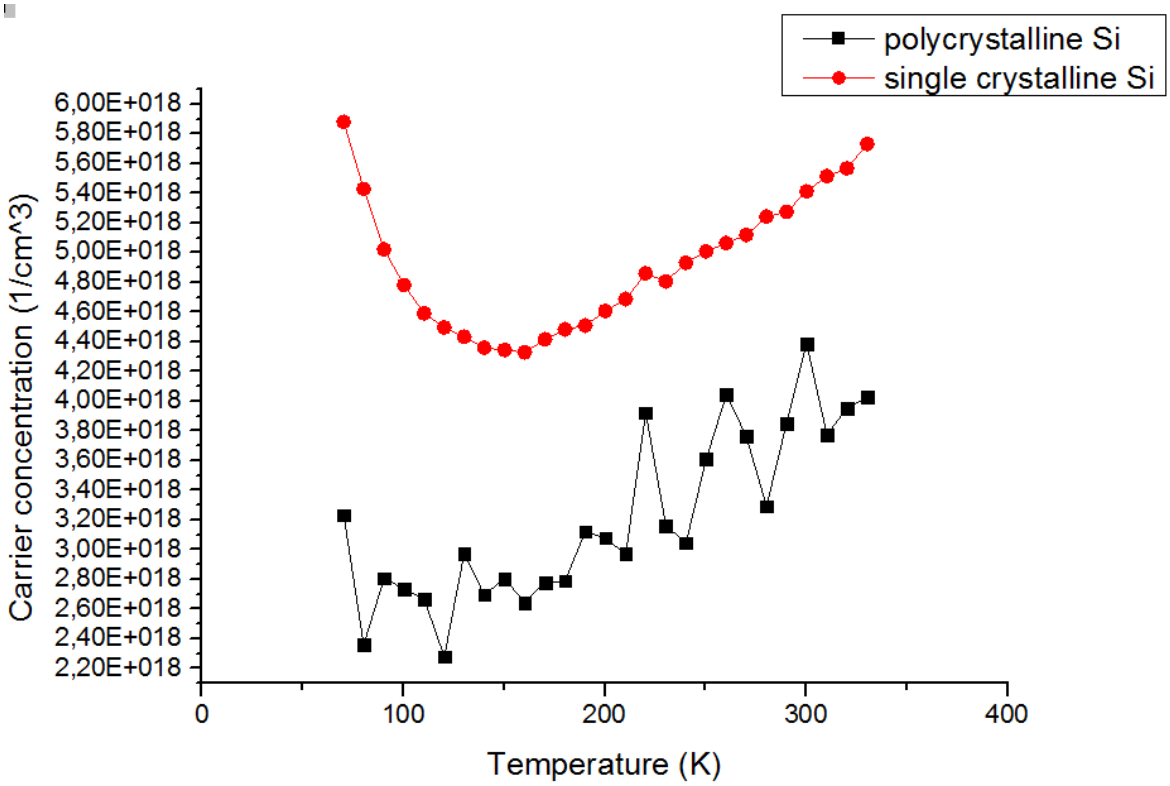

Figure 6.13: The carrier concentrations of the polycrystalline and the single crystalline silicon samples.

The properties of the polycrystalline sample were actually measured starting from the temperature of 10 K. However, between 10 K and 70 K the Hall coefficient was changing its sign, depending on the sign of the magnetic field. The *V(I)* curves were rather non-linear, as seen in figure 6.14. Both these factors got better around 70 K. The Hall coefficient stopped changing its sign, and the IV-curves got slightly more linear.

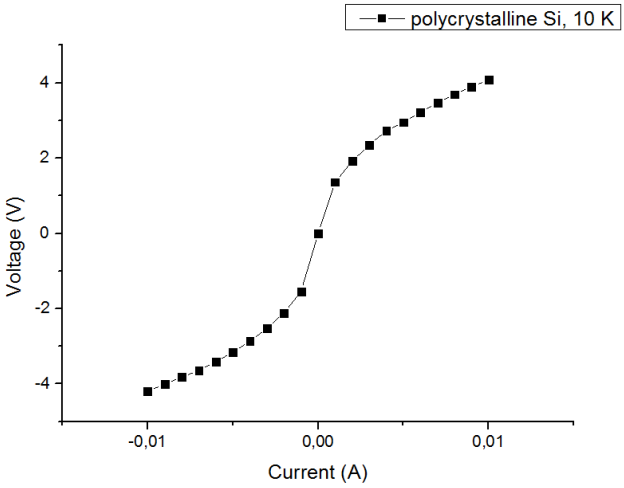

Figure 6.14: A typical IV-curve at temperature 10K.

6.4.3 Seebeck coefficient

The Seebeck voltage of the single crystalline sample is plotted in figure 6.15. The measurement points are rather large, and make the graphs look thick. The first minimum and maximum correspond to measurements at 50°C. The second minimum and maximum correspond to measurements at 100°C. Using the method proposed in chapter 4, The Seebeck coefficient vs. *T* graphs were found (figure 6.16).

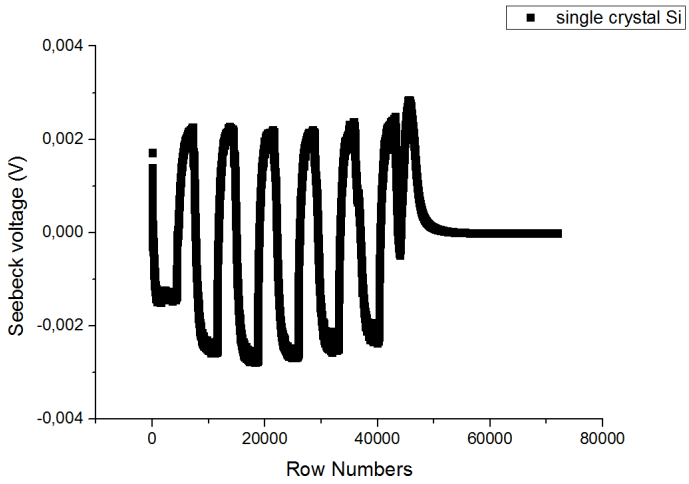

Figure 6.15: Seebeck voltage of single crystalline silicon sample, vs. numbers

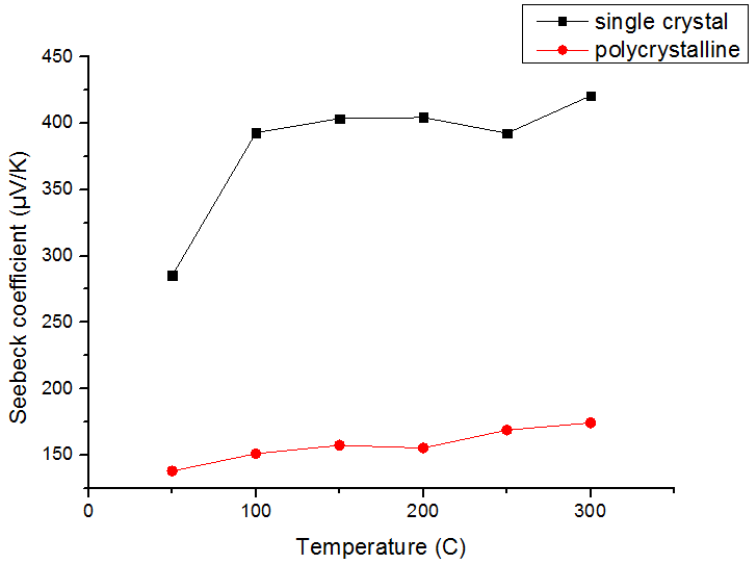

Figure 6.16: The Seebeck coefficients of the polycrystalline and single crystalline samples.

Chapter 7

Discussion

In this chapter, results are combined and discussed. Important details are emphasized.

7.1 Synthesis of polycrystalline silicon

The rule of thumb is that sintering temperature for an element should be around two thirds of its melting temperature. For silicon, melting temperature is 1414°C, which would make its sintering temperature around 943°C. However, the failure of the sintering synthesis at 1000°C contradicted the expectations. It is possible the sintering temperature was much higher than expected, because the fine powder became oxidized before sintering, and got covered with silicon dioxide. However, EDS results did not detect any oxygen. It did, however, detect a little iron. It could come from the various polishing and cutting instruments. But it could also mean that using a steel cup and steel balls for ball-milling introduced contamination.

As predicted by the literature, it was hard to obtain a dense sample with the sintering technique[ref4]. The density of the sintered sample is ca. 15-22% lower than of the single crystalline silicon.

7.2 Density and porosity determination of the polycrystalline Si sample

Results of porosity determination varied widely. The geometric method gave larger porosities, while the Archimedes method gave smaller porosities. If one looks at the equations that give the Archimedes porosity, several factors could be making the porosity smaller than expected. Density of water used in the calculations ρ_w and M_{water} could be too large. Density of silicon ρ_{Si} could be too small. ρ_w used in calculations could be too large, if the temperature of water was incorrectly found to be lower than it was. Density of silicon ρ_{Si} was imagined to be the density of the solid part of the sample, minus the pores. However, if the sample contains a big amount of silicon dioxide, the density could be larger. The density of silicone dioxide is 2.648 g/cm^3, while the density of pure single crystal silicon is 2.329 g/cm^3.

However, none of these things would make as much difference as the phenomenon of the samples quickly soaking up water. The fact that the samples soak up water can be easily

observed. When placed on the scale after prolonged contact with water, a sample seems to lose mass. It also seems to gain mass rather quickly when weighed in water.

If the difference in porosity is due to the soaking up of water, then the pores must be extending deep into the sample, most likely connected into channels. Superficial pores would not take up any water that would make such a difference. If this assumption is right, then it is also reasonable to assume that when the sample is quickly immersed in water, the water will enter the channels. Capillary forces would pull it deeper into the sample from all its sides, until it was stopped by the air, trapped in the middle of the sample. It would have nowhere to go. However, if the sample is slowly immersed in water, the water will enter from the bottom side only, and force out the air from the top side. Thus, a smaller calculated porosity could mean the sample was immersed slower, and higher calculated porosity could mean the sample was immersed quicker.

Since EDS didn't detect any oxygen at any spot, it's unlikely that silicon dioxide is the cause of the disparity between results of the geometrical and the Archimedes methods.

7.3 Characterization of the microstructure

Both optical and scanning electron microscopy showed that a polished flat surface is covered with small holes. Coupled with the results of porosity measurements, it indicates that the sample is most likely porous. There are, of course, other possibilities. It is possible the sample is relatively brittle, and small chunks of material fall off when the surface is polished. However, the holes appear not only along the polish lines, but also in the middle of otherwise smooth areas.

The size of the holes in the surface varies. Many are a few µm in diameter, while others are smaller. The optical microscopy has shown that it is possible to look inside some of these holes, and estimate the depth. They were often 4-25 µm deep, which helped support the hypothesis that the pores reach deep into the sample and perhaps are connected into channels.

Characterization with TEM has shown that the grains of the sample tend to exceed the nanoscale. Many are several µm in diameter. The material produced is therefore not a hybrid material. Its pores and air inclusions also appear to be rather large. The TEM sample also had many holes in it. It is hard to determine if these holes are the original pores, formed during sintering, or formed during the ion milling process. If holes in the TEM sample represent the

original pores, it is hard to determine if the sizes seen on the TEM pictures are original. Ion milling could have modified the pores and made them look bigger. Ion milling also tends to mill away material at the grain boundaries first. Then a grain can eventually fall out, and form a false pore.

7.4 Thermoelectric properties

7.4.1 Resistivity

Resistivity of the polycrystalline sample is somewhat higher than that of the single crystalline sample. It is an expected result, as conductivity of a thermoelectric often tends to decrease with introduction of grain boundaries. Grain boundaries, especially incoherent ones, scatter charge carriers. Another possible reason for the reduction in conductivity is the introduction of air-filled pores. Air is a poor electrical conductor.

Both resistivities also decrease with temperature, and become constant somewhere between 260K and 0°C. It is an expected result as well. A cold semiconductor is often said to be a useless conductor. The low temperature implies a low thermal energy supplied to the charge carriers. Very few electrons can jump from the valence band to the conduction band. And at very low temperatures, the holes can’t even jump from the acceptor levels created by the dopant, to the valence band. With increasing temperature, charge carriers receive more thermal energy, and therefore more of them participate in conduction.

7.4.2 Carrier concentration

Carrier concentration of the polycrystalline sample is roughly cut in two, compared to that of the single crystalline sample. One explanation is that the energy filtering effect has worked, and stopped the carriers with lowest energies.

For both, the carrier concentration drops, and then starts to rise again, at 100K for polycrystalline and around 150K for single crystalline sample. The rising carrier concentration was already explained in part 7.4.1. Rising temperature gives more energy to the carriers, and more of them can overcome the energy boundary that is stopping them from participating in conduction.

7.4.3 Hall mobility

The Hall mobility of the polycrystalline sample was lower than that of the single crystalline silicon sample. As mentioned in chapter 4, complete removal of oxide layers is necessary for producing a good polycrystalline thermoelectric through the sintering method. However, no oxygen was detected in the polycrystalline sample by EDS, and it is not likely to be the reason for the reduced mobility.

Another possible reason the mobility has been reduced is the rough, incoherent interfaces between the grains. It is known that the sintering process creates such interfaces, and that they are strong scatterers of electrons.

Another possibility is the presence of amorphous silicon. Could the ball milling process create amorphous material in the polycrystalline sample? [13]. Some studies indicate that even ball-milling for 30 minutes can broaden the diffraction peaks of an X-ray diffraction pattern of a powder sample. That could mean amorphous phases are appearing. Broadening of peaks also means the grains are becoming smaller. Amorphous material is not the easiest material for a charge carrier to move through.

Both graphs on figure… also increase with temperature, before starting to decline around 225K (-48°C). The temperature-dependence of mobility can be written as $\mu \propto T^r$, where r is a scattering parameter. It takes different values, depending on scattering mechanisms. It is possible that the change in the slope of the $\mu(T)$ graph means scattering mechanism has changed at that specific temperature.

7.4.4 Thermal conductivity

The thermal conductivity of the polycrystalline sample was slightly lower than that of the single crystal sample at almost all temperatures. It fits with the knowledge that the sample was porous, and air is a poor thermal conductor. On the other hand, the grains of the polycrystalline sample were not generally on the nanoscale, which could have made the reduction in κ less than it could have been. Smaller grains would mean shorter phonon mean free path.

Both thermal conductivities are reduced with temperature.

7.4.5Seebeck coefficient

A positive Seebeck coefficient is expected, as the samples are all made of a p-type semiconductor. It is also expected that it would be larger for the polycrystalline material, in consistency with the carrier concentration measurements. However, this is not so. The Seebeck coefficient of the polycrystalline sample is smaller than that of the single crystal sample. It is possible air inclusions played their part. It appears unlikely that air would be able to produce a useful thermoelectric voltage. It is a poor conductor. It is also possible the instrument was not able to measure the Seebeck voltages of the single crystal Si correctly. The sample was, after all, very thin.

Chapter 8

Conclusion

This work has shown that two thirds of the melting temperature was not enough to sinter a silicon powder into a solid material. However, 1300°C, only 114°C away from the melting point, achieved that task. The synthesis method of ball-milling and sintering induces surprisingly little oxidation of the silicon, even if both are not done under vacuum or specialized inert atmosphere. However, the method did not produce a very dense sample. The porosity was likely between 15 and 22%. The pores were most likely interconnected and had an average diameter of 1-3 µm. The grains were also of a similar size on average, which means the material can't be considered a hybrid material of silicon and air-filled pores.

Introduction of polycrystallinity and pores have many netative effects on the boron-doped silicon. The resistivity increased likely both due to introduction of air inclusions, and due to increased amount of grain boundaries. The latter also decreased carrier mobility as expected. The carrier concentration was also decreased, possibly by the energy-filtering effect. Surprisingly, the Seebeck coefficient was also decreased. The only positive effect was the slight reduction in thermal conductivity, likely due to increased phonon scattering.

The effective medium theories are many, and each fits a certain range of criteria. Each requires good microstructural characterization and other important knowledge about the material. Most often, the model chosen to describe the material will mean either apparent failure or success of the EMT.

Chapter 9

Suggestions for further work

Many things could have been done differently in this thesis work, to obtain better results.

The polycrystalline material was not a nanocomposite. Some articles suggest ball-milling the materials for up to 92 hours to achieve nanocrystal powder. Perhaps that would have helped achieve nanocrystallinity, and possibly better thermoelectric properties.

Perhaps the material could have been tested for stability. During the measurements of electrical properties, the material was heated to high temperatures, such as 300°C and 650°C. It could have changed the grain sizes, allowing big grains to grow at the expense of the small ones.

Measuring the volume of the sample was challenging, as it was very porous and the Archimedes method yielded many different results. A gas pycnometer could perhaps be a better choice. One could also synthesize many samples with the exact same method, and measure their porosities with the geometric method. It would give a range of porosities, from which an average could be found. Perhaps then a much more precise value for porosity could have been found.

It would have been interesting to see how an EMT would predict the effective thermoelectric properties as a function of air inclusion content. Many other studies have done this, and it shows a good picture of whether an EMT is valid or not. An EMT, per definition, is a function for an effective property, which varies with inclusion volume fraction. Thus, it would be a good study to measure effective thermoelectric properties as functions of phase content, ball milling time and perhaps other synthesis parameters that affect phase content.

Bibliography

[1] J. Rekstad, M.M., *Energy and Physics*. 2012.

[2] Bux, S.K., et al., *Mechanochemical synthesis and thermoelectric properties of high quality magnesium silicide.* Journal of Materials Chemistry. **21**(33): p. 12259-12266.

[3] Goldsmid, H.J., *Introduction to Thermoelectricity*. Springer Series in Materials Science, ed. J.P. R. Hull, R. M. Osgood Jr., H. Warlimont. 2010: Springer.

[4] Snyder, G.J. and E.S. Toberer, *Complex thermoelectric materials.* Nature Materials, 2008. **7**(2): p. 105-114.

[5] Dresselhaus, M.S., et al., *New directions for low-dimensional thermoelectric materials.* Advanced Materials, 2007. **19**(8): p. 1043-1053.

[6] Kanatzidis, M.G., *Nanostructured Thermoelectrics: The New Paradigm?* Chemistry of Materials. **22**(3): p. 648-659.

[7] M.C. Lovell, A.J.A., M.W. Vernon, *Physical Properties of Materials*. 1976: Van Nostrand Reinhold Company Ltd.

[8] *CRC Handbook of Thermoelectrics*, ed. D.M. Rowe. 1995.

[9] *Hybrid Materials: Synthesis, Characterization, and Applications*, ed. G. Kickelbick. 2007: WILEY-VCH Verlag GmbH & Co. KGaA.

[10] *Hybrid Nanomaterials: Synthesis, Characterization, and Applications*, ed. B.P.S. Chauhan. 2011: John Wiley & Sons, Inc.

[11] Liu, W., et al., *Recent advances in thermoelectric nanocomposites.* Nano Energy. **1**(1): p. 42-56.

[12] Poon, S.J. and K. Limtragool, *Nanostructure model of thermal conductivity for high thermoelectric performance.* Journal of Applied Physics. **110**(11): p. 7.

[13] Kyratsi, T., et al., *Seebeck and thermal conductivity analysis in amorphous/crystalline beta-K2Bi8Se13 nanocomposite materials.* Journal of Applied Physics. **110**(3).

[14] Frank J. Owens, C.P.P.J., *The Physics and Chemistry of Nanosolids*. 2008: John Wiley & Sons, Inc.

[15] Choy, T.C., *Effective Medium Theory: Principles and Applications*. 1999: Oxford University Press Inc.

[16] Das, P.K., X.G. Li, and Z.S. Liu, *Effective transport coefficients in PEM fuel cell catalyst and gas diffusion layers: Beyond Bruggeman approximation.* Applied Energy. **87**(9): p. 2785-2796.

[17] Sharma, P.A., J.D. Sugar, and D.L. Medlin, *Influence of nanostructuring and heterogeneous nucleation on the thermoelectric figure of merit in AgSbTe2.* Journal of Applied Physics. **107**(11).

[18] Lee, J., et al., *Phase purity and the thermoelectric properties of Ge2Sb2Te5 films down to 25 nm thickness.* Journal of Applied Physics. **112**(1).

[19] Zaitsev, V.K., et al., *Highly effective Mg2Si1-xSnx thermoelectrics.* Physical Review B, 2006. **74**(4): p. 5.

[20] Du, Y., et al., *Research progress on polymer-inorganic thermoelectric nanocomposite materials.* Progress in Polymer Science. **37**(6): p. 820-841.

[21] Stoecker, T., A. Koehler, and R. Moos, *Why does the electrical conductivity in PEDOT:PSS decrease with PSS content? A study combining thermoelectric measurements with impedance spectroscopy.* Journal of Polymer Science Part B-Polymer Physics. **50**(14): p. 976-983.

[22] Hurvits, G., R. Rosenbaum, and D.S. McLachlan, *A QUANTITATIVE-ANALYSIS OF THE THERMOELECTRIC-POWER MEASUREMENTS ON COMPOSITE AL-GE FILMS.* Physica A, 1994. **207**(1-3): p. 391-395.

[23] Hao, F., D. Fang, and Z. Xu, *Thermal transport in crystalline Si/Ge nano-composites: Atomistic simulations and microscopic models.* Applied Physics Letters. **100**(9).

[24] P. Kofstad, T.N., *Defects and Transport in Crystalline Solids*. 2012.

[25] H. D. Young, R.A.F., *University Physics*. Pearson International Edition, 12th ed. 2008: Pearson Addison-Wesley.

[26] D. Brandon, W.D.K., *Microstructural Characterization of Materials*. 2nd ed. 2008: John Wiley & Sons Ltd.

[27] M. A. Tupta, *Instrumentation and Techniques for Measuring High Resistivity and Hall Voltage of Semiconducting Materials*. 2005, Keithley Instruments, Inc.

[28] Schroder, D.K., *Semiconductor Material and Device Characterization*. 3rd ed. 2006: John Wile & Sons, Inc.

[29] *Lake Shore 7500/9500 Series Hall System User's Manual*, Lake Shore Cryotronics, Inc.

[30] *LFA 457 MicroFlash*. [cited 2013 4.05]; Available from: http://www.netzsch-thermal-analysis.com/uploads/tx_nxnetzschmedia/files/LFA_457_E_0413.pdf .

[31] *Springer Materials The Landolt-Bornstein Database*.

[32] [cited 2013 5.05]; Available from: http://uio.norfab.no/WebForms/Equipment/EquipmentView.aspx?toolId=8.

Appendix

A.1 List of selected symbols

∇T	Temperature gradient
ΔT	Temperature difference
α	Seebeck coefficient
V	Voltage
α_{AB}	Relative Seebeck coefficient, materials A and B
α_A	Seebeck coefficient of material A
π_{AB}	Relative Peltier coefficient, materials A and B
I	Electric current
J	Electrical current density
ZT	Figure of merit
σ	Electrical conductivity
κ	Thermal conductivity
$\alpha^2\sigma$	Power factor
κ_{latt}	Lattice thermal conductivity
κ_e	Electric thermal conductivity
ρ	Resistivity, or mass density
n	Charge carrier concentration (n-type material)
p	Charge carrier concentration (p-type material)
μ	Charge carrier mobility
μ_e	Electron mobility
μ_h	Hole mobility
μ_H	Hall mobility
m^*	Effective carrier mass
k_B	Boltzmann's constant
L	Lorentz number
v	Phonon velocity
λ	Phonon mean free path
c, c_p	Specific heat capacity
r	Scattering parameter

ε	Dielectric constant
ε_i	Dielectric constant of the inclusions, or phase *i*
ε_{mat}	Dielectric constant of the matrix phase
f_i	Volume fraction of phase *i*, or of the inclusions
f_c	Critical threshold
σ_i	Electrical conductivity of phase *i*, or of inclusions
κ_i	Thermal conductivity of phase *i*, or of inclusions
α_i	Seebeck coefficient of phase *i*, or inclusions
σ_{eff}	Effective electrical conductivity
κ_{eff}	Effective thermal conductivity
α_{eff}	Effective Seebeck coefficient
E_x	Electric field in the x-direction
R_H	Hall coefficient
B_z	Magnitude of the magnetic field in the z-direction
M_{air}	Weight of sample in air
T_w	Temperature of water
ρ_w	Mass density of water
$M+_{air}$	Mass of (table + copper wire + sample), in air
$M+_{water}$	Apparent mass (table + copper wire halfway in water + sample in water)
ρ_{Cu}	Mass density of copper at room temperature
$M_{cu,w}$	Mass of copper wire that went underwater (in air)
ρ_{Si}	Density of pure single crystal silicon at 25°C